Award Number: W81XWH-07-1-0215

TITLE: Cellular Therapy to Obtain Rapid Endochondral Bone Formation

PRINCIPAL INVESTIGATOR: Elizabeth A. Olmsted-Davis, Ph.D.

CONTRACTING ORGANIZATION: Baylor College of Medicine
Houston, TX 77030

REPORT DATE: March 2012

TYPE OF REPORT: Final Addendum

PREPARED FOR: U.S. Army Medical Research and Materiel Command
Fort Detrick, Maryland 21702-5012

REPORT DOCUMENTATION PAGE

Form Approved
OMB No. 0704-0188

1. REPORT DATE *(DD-MM-YYYY)*	2. REPORT TYPE	3. DATES COVERED *(From - To)*
01-03-2012	Final Addendum	1 Feb 2007 - 28 Feb 2012

4. TITLE AND SUBTITLE

Cellular Therapy to Obtain Rapid Endochondral Bone Formation

5a. CONTRACT NUMBER

5b. GRANT NUMBER

W81XWH-07-1-0215

5c. PROGRAM ELEMENT NUMBER

6. AUTHOR(S)

Elizabeth A. Olmsted-Davis, Ph.D.

E-Mail: edavis@bcm.edu

5d. PROJECT NUMBER

5e. TASK NUMBER

5f. WORK UNIT NUMBER

7. PERFORMING ORGANIZATION NAME(S) AND ADDRESS(ES)

Baylor College of Medicine
Houston, TX 77030

8. PERFORMING ORGANIZATION REPORT NUMBER

9. SPONSORING / MONITORING AGENCY NAME(S) AND ADDRESS(ES)

U.S. Army Medical Research and Materiel Command
Fort Detrick, Maryland 21702-5012

10. SPONSOR/MONITOR'S ACRONYM(S)

11. SPONSOR/MONITOR'S REPORT NUMBER(S)

12. DISTRIBUTION / AVAILABILITY STATEMENT

Approved for Public Release; Distribution Unlimited

13. SUPPLEMENTARY NOTES

14. ABSTRACT

The goal of this study is to provide a safe effective system for inducing bone formation for fracture healing in situations of significant trauma. This set of proposed experiments will provide significant knowledge to the field of bone tissue engineering. Proposed studies will provide essential biological information and involves the development of a novel biomaterial that can safely house the cells expressing the bone inductive factor to produce the new bone at which time the material is then selectively eliminated. Ultimately this system has significant applicability. Often bone graft must be surgically removed from the pelvis, to implant into the site of difficult fractures for proper healing. This additional surgery often results in significant pain, and long term healing. Further, this system would be applicable to orthopedic trauma situations that previously resulted in amputation. We propose in these studies to complete the development of this bone induction system and test it in a preclinical animal model. Validation of our hypothesis will provide a safe and efficacious material for the production of bone leading to reliable fracture healing, circumventing the need for bone grafts, or for direct administration of cells, viruses, or other materials that could lead to significant adverse reactions.

15. SUBJECT TERMS

BMP2, hydrogel, critical size defect, nonunion, gene therapy, adenovirus.

16. SECURITY CLASSIFICATION OF:			17. LIMITATION OF ABSTRACT	18. NUMBER OF PAGES	19a. NAME OF RESPONSIBLE PERSON
a. REPORT	b. ABSTRACT	c. THIS PAGE			USAMRMC
U	U	U	UU	34	19b. TELEPHONE NUMBER *(include area code)*

Table of Contents

Introduction: This project, on the use of cell-based gene therapy for the production of rapid endochondral bone formation, and fracture healing is a collaborative effort between a bio-engineering/biomaterials group at Rice University and Baylor College of Medicine. Although bone possesses the rare capacity to continually renew and repair itself, more than 500,000 bone repair surgical procedures are performed annually within the United States alone. The need to enhance or initiate bone formation in a controlled clinical manner has brought tissue engineering to the forefront of orthopedic research. Much recent effort has been directed to the identification of factors essential to normal bone formation, and the development of new osteoconductive materials that can temporarily fill areas of missing osteoid. Still lacking are effective osteoinductive components that could be seeded into the osteoconductive materials to generate normal bone which this study will explore. The central hypothesis of this application is that rapid bone formation can be successfully achieved with only minimally invasive percutaneous techniques and without a scaffold, by using cells transduced with adenovirus vectors to express an osteoinductive factor (BMP2), which have been encapsulated in hydrogel material and later photopolymerized at the desired site.

The goal of this study is to provide a safe effective system for inducing bone formation for fracture healing. This set of proposed experiments will provide significant knowledge to the field of bone tissue engineering. Proposed studies will provide essential biological information and involves the development of a novel biomaterial that can safely house the cells expressing the bone inductive factor to produce the new bone at which time the material is then selectively eliminated. Ultimately this system has significant applicability. Often bone graft must be surgically removed from the pelvis, to implant into the site of difficult fractures for proper healing. This additional surgery often results in significant pain, and long term healing. Further, this system would be applicable to orthopedic trauma situations that previously resulted in amputation. We propose in these studies to complete the development of this bone induction system and test it in a preclinical animal model. Validation of our hypothesis will provide a safe and efficacious material for the production of bone leading to reliable fracture healing, circumventing the need for bone grafts, or for direct administration of cells, viruses, or other materials that could lead to significant adverse reactions.

Body: The central hypothesis of this application is that rapid bone formation can be successfully achieved with only minimally invasive percutaneous techniques and without a scaffold, by using cells transduced with adenovirus vectors to express an osteoinductive factor (BMP2), which have been encapsulated in hydrogel material and later photopolymerized at the desired site.

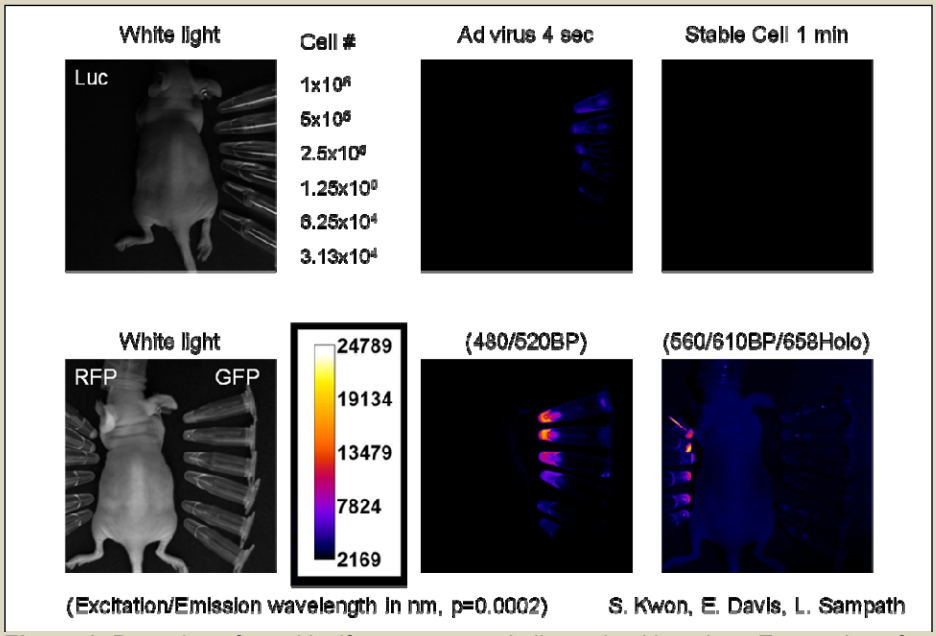

Figure 1: Detection of a red luciferase reporter in live animal imaging. Expression of a red shifted luciferase reporter was compared both in cells, and in live animals after subcutaneous intramuscular injection.Two types of cells were tested, one which was a cell line that had the reporter stably integrated, and the other cells which had been transduced with an AdCRBluc virus.

Task 1: *To determine the optimal levels of BMP2 for efficient rapid production of endochondral bone from human bone marrow mesenchymal stem cells (hBM-MSCs) transduced with a tetracycline regulated Ad5F35tet-BMP2 adenovirus carrying a red luciferase reporter gene.*

a. To determine if sustained expression of BMP2 is more efficient at inducing rapid bone formation than a pulse of expression using the tetracycline regulated vectors. **(Months 0-12)** Comparison studies were performed to determine the optimal method for tracking transgene expression *in vivo*.

As seen in figure 1, the originally described methodology using red luciferase reporter gene expression was compared to other red-shifted reporters to determine if we could obtain something more sensitive which would allow us to image the expression of the transgene during bone formation. In original experiments using luciferase (figure 1) we were unable to readily detect the reporter after intramuscular injection of our transduced cells at the levels routinely used for induction of bone formation. However, as seen in figure 2, when this was compared to dsRED, a red fluorescent protein, we could readily detect dsRED. Therefore we initiated studies using dsRED in place of the red luciferase.

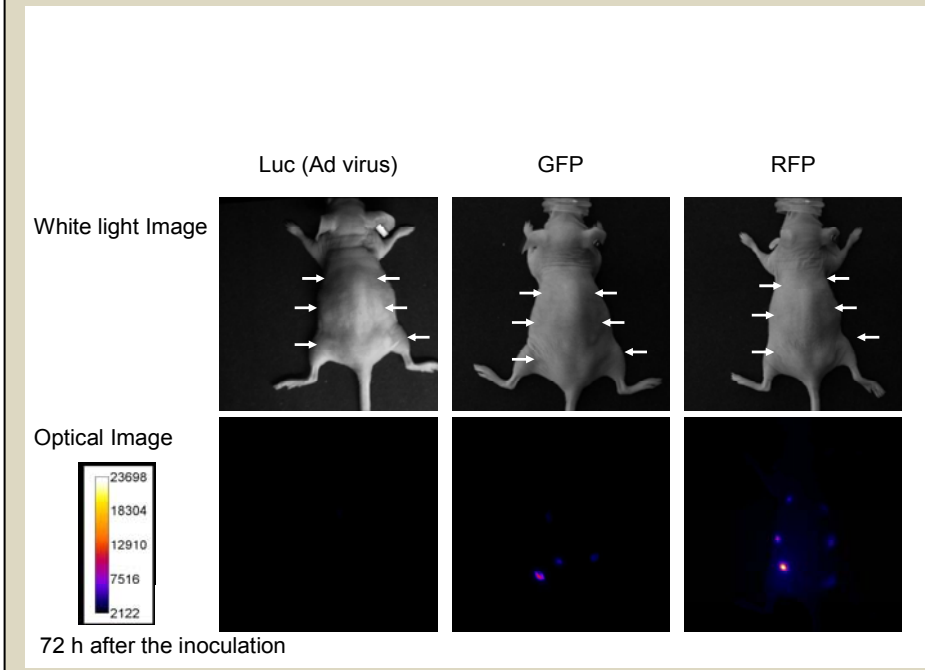

Figure 2: Comparison of reporter expression after intramuscular injection of dsRED, GFP, and CRBluc in live animals, through optical imaging.

In these studies, cells were transduced with Ad5dsRED (2500 vp/cell) and were encapsulated into microbead structures using PEGDA hydrogel (nondegradable). The microbeads were then injected into the hindlimbs of the animal, and transgene expression compared to animals receiving the same Ad5dsRED transduced cells which have not been encapsulated.

Two days after the initial injection of cells, dsRED expression was readily detected whether cells were encapsulated or not and in no cases were cells or microspheres detected migrating from the injection site (Figure 3A). The dsRED expression, as measured by fluorescence intensity at 590 ± 10 nm, was significantly elevated in microencapsulated Ad5dsRED-transduced cells compared to other groups (Figure 3B). Microencapsulated control cells transduced with AdEmpty cassette had no fluorescent signal at 590 ± 10 nm, demonstrating that neither the cells nor the PEGDA were autofluorescing. Fluorescent intensity in animals receiving Ad5dsRED-transduced cells directly injected was substantially reduced after seven days and was indistinguishable from control. In microencapsulated Ad5dsRED-transduced cells, this 590 ± 10 nm dsRED fluorescent signal was significantly elevated over that of microencapsulated control cells for 15 days (Figure 3B). After 15 days, these levels dropped; however, signal was still detectable (Figure 3A, arrows) in some animals, suggesting that the microencapsulated cells remained viable to express the dsRED transgene. Statistical power to detect intensity over control ranged from 100% in microencapsulated cells to 99.7% in directly injected cells, and power to detect the difference between microencapsulated and unencapsulated cells was 88%.

Through these imaging experiments we are able to use dsRED to analyze bone formation after delivery of BMP2 short term or long term. **See following section.**

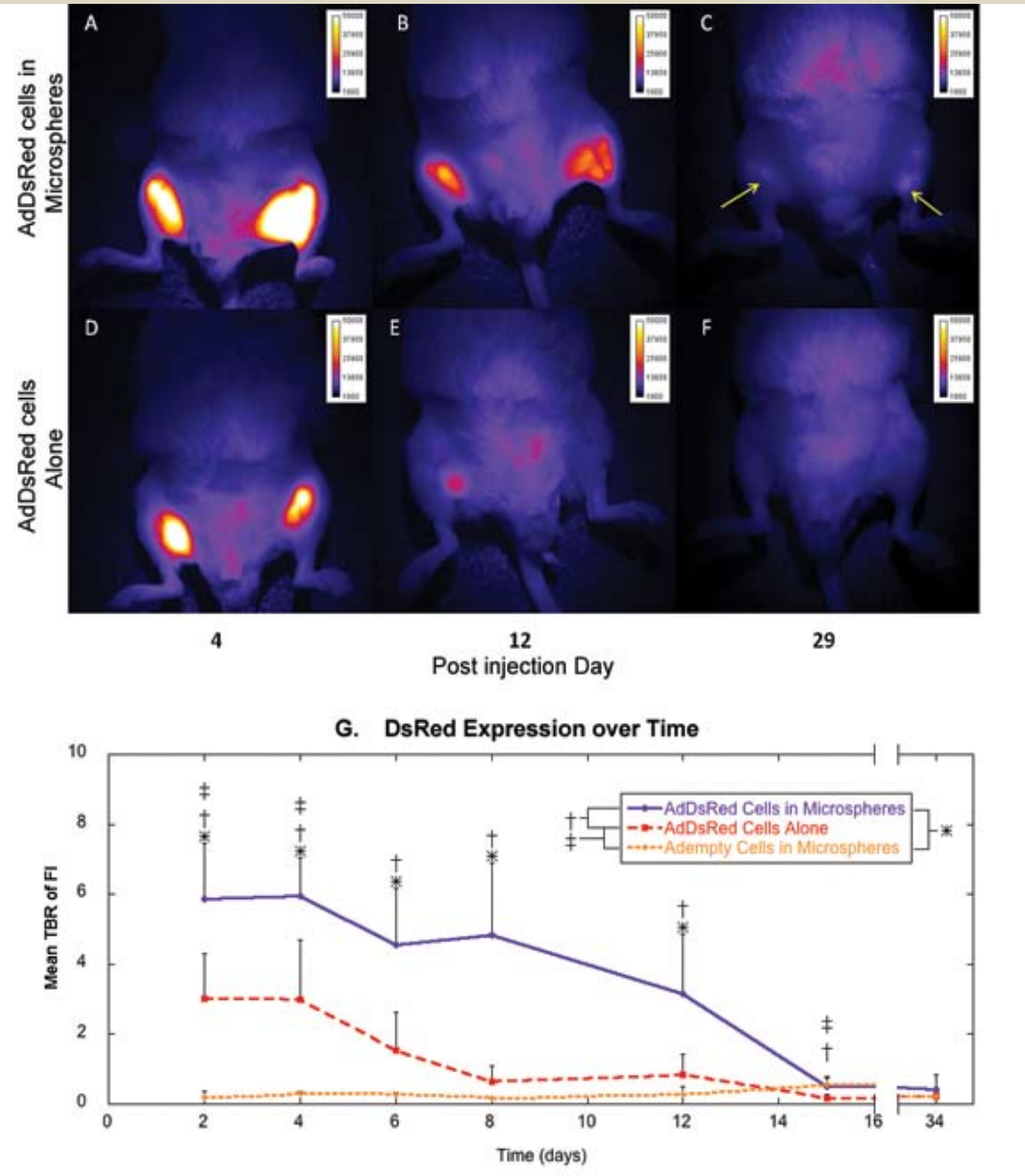

Figure 3: Optical fluorescence imaging of mice injected with cells expressing dsRed. Top panels (A through C) are images of a representative mouse (n=4) injected with dsRed-expressing cells encapsulated in microspheres and bottom panels (D through F) are of a mouse injected with dsRed-expressing cells directly, without microspheres. The images were taken at day 4, 12 and 29 post-injection of cells. By day 29, the fluorescent signal is at background levels or undetectable for the mouse given dsRed-expressing cells without microspheres (F). Whereas, the signal remains detectable in the mouse given dsRed-expressing cells encapsulated in microspheres (C).
G. Mean Target-to-Background Ratio (TBR) of Fluorescence Intensity (FI) in mice given unencapsulated dsRed cells, microencapsulated dsRed cells or microencapsulated control cells. * $p \leq 0.05$ for microencapsulated dsRed cells versus microencapsulated control cells; † $p \leq 0.05$ for microencapsulated dsRed cells versus unencapsulated dsRed cells; ‡ $p \leq 0.05$ for unencapsulated dsRed cells versus microencapsulated control cells.

b. ***To determine if longer expression times of BMP2 from cells embedded in hydrogel and longer cellular viability lead to more rapid bone formation than the rapid but short burst of BMP2 release obtained from the cells directly injected. (Months 9-12)***

We next set up similar experiments to track the dsRED in live animals during heterotopic ossification. In these experiments, we transduced the cells with an Ad5BMP2-dsRED virus, which was not tetracycline regulated. In these studies we look at the ability to detect the signal through the bone matrix that is forming. As seen in figure 4, dsRED could readily be detected above background for up to 16 days. Interestingly, the cells directly injected appeared to be readily detected, and stronger than the cells within the microbeads. Both the microbeads and directly injected cells were tracked up to 16 days, again which is odd, considering all previous experiments appeared to remove the cells rapidly after 6 -8 days. The data does suggest that we can track the reporter even in the presence of bone formation. Further, the signal is stronger in the directly injected cells, most likely because the microbeads, and bone itself that is forming, shield the signal as compared to the directly injected cells that are not necessarily encapsulated within the bone. Further, the bone formation as determined by micro CT was not as robust in the samples receiving the cells directly, thus less shield would also occur.

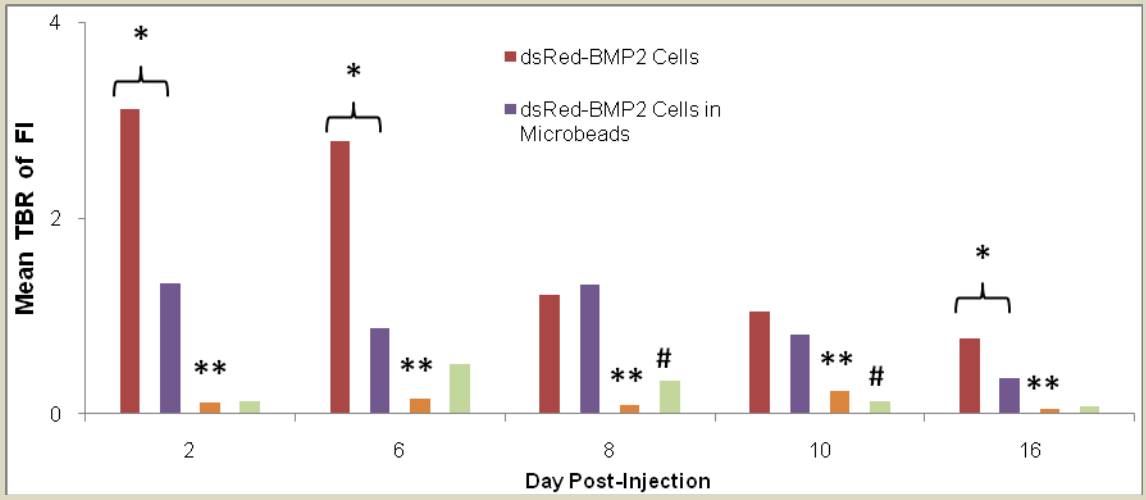

Figure 4: Mean Target-to-Background Ratio (TBR) of Fluorescence Intensity (FI) in mice given unencapsulated dsRed cells, microencapsulated dsRed cells or microencapsulated control cells.
*P < 0.05 for Ad5dsRED-BMP2 transduced cells versus Ad5dsRED-BMP2 cells in microbeads at days 2, 6, and 16 post-injection.
**P < 0.05 for Ad5dsRED-BMP2 cells transduced cells versus Ad5dsRED-BMP2 cells in microbeads at all time points.
# P < 0.05 for dsRED-BMP2 cells in microbeads versus Ad5empty cassette transduced cells (Control) in microbeads at days 8 and 10 after injection.

In these live animal imaging experiments we determined that the hydrogel greatly increased the length of expression time of the BMP2. Further, although the when similar numbers of cells are encapsulated in hydrogel microspheres (See Task 2), led to 3 fold more bone than was obtained when these cells were directly injected, the pattern of the new bone, suggested that this may be in part because the area of BMP2 expression was much greater, due to the addition of the polymer whereas the cells directly injected clumped between the muscle fibers and were encompassed a much smaller region. Further, dose curves done in rats (see Task 3) clearly show that there is a maximum amount of bone that can be obtained, and adding more BMP2 did not lead to a greater effect, presumably because the receptors may be saturated. ***This work has been published in Olabisi, R. et al, Tissue Engineering Part A. Dec 2010, 16(12):3727-36 and Lazard, Z.W. et al, J Cellular Biochemistry, In press).*** ***These two sub-aims are completed.***

c. To demonstrate the termination of BMP2 expression using an Ad5F35tet-BMP2-IRESCBRLuc vector in which expression can be tracked through live animal imaging. ***(Months 12-24). See above section.***

d.To determine what the responder cells to the BMP2 are proximal or more distal to the hydrogel encapsulated delivery cells by performing live animal confocal imaging which follows the translocation of a Smad 1 to the nucleus. ***(Months 24-48)***

We have performed extensive studies to determine if the reaction is systemic or local and have identified key tissues that are responding to the BMP2 to mobilize stem cells for new bone. In these studies we have found that sensory peripheral nerves play a key role in this process, as well as local stem and progenitors. We have focused on idenfitying these local cells in this aim.

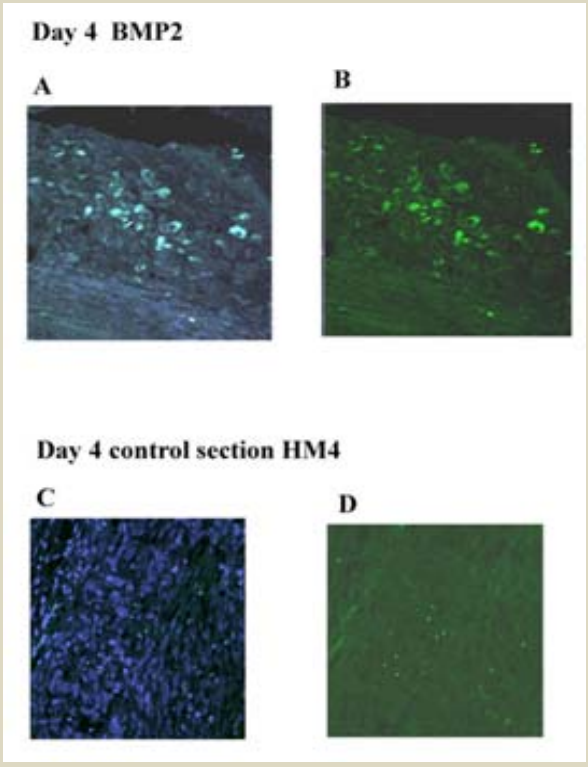

Figure 5: Immnuno-fluorescence staining on tissues isolated four days after receiving Ad5F35BMP2 transduced cells (A and B) or cells transduced with a control virus Ad4F35HM4 (C and D). Sections B and D are stained with Phospho-Smad1/5/8 antibody (1/100 dilution, Cell Signaling technology) and a secondary antibody anti-rabbit Alexa Fluor 488 conjugated. Sections A and C and stained with Phospho-Smad1/5/8 and counterstained with DAPI

could be one of the earliest responding cells to the BMP2.

Previous work in the literature suggests that the nerves respond by inducing neuroinflammation through the secretion of substance P and CGRP proteins. To determine if BMP2 directly activates expression of the neuroinflammatory proteins SP and CGRP during heterotopic ossification, proteins were isolated from tissues at daily intervals, starting 24 hours after delivery of AdBMP2 or Adempty (control virus) transduced cells, through the appearance of heterotopic bone. Quantification of protein levels of SP and CGRP within the tissues, through ELISA, is shown in figure 6A and B, respectively. Both proteins appear to be significantly elevated ($p \leq 0.0005$), compared to controls, within 24 hours after induction of HO, and again at 72 hours ($p \leq 0.005$) and 6 days ($p \leq 0.05$) after induction. Expression, therefore, appeared somewhat cyclical, and statistical analyses, using a one-way ANOVA

We generated the proposed mouse line, but were unable to detect the YFP expression most likely due to the nature of smad expression. This is a low copy number protein and without additional amplification, as with immunostaining, the expression was below the level of detection. We next switched the YFP to cyanin fluorescent protein and red fluorescent protein; neither provided high enough expression within the nucleus to provide unequivocal data. Therefore we went ahead and did some immuno staining with an antibody specific to phosphoSmad (figure 5). We localized positive expression to several cell types, however, in tissue sections isolated at 24 hours after delivery of BMP2, the expression was found associated with the peripheral nerves whereas, tissues receiving the control cells had no positive expression. Since BMP2 had previously been shown to have direct effects on peripheral nerves in culture, we next determined whether the nerve

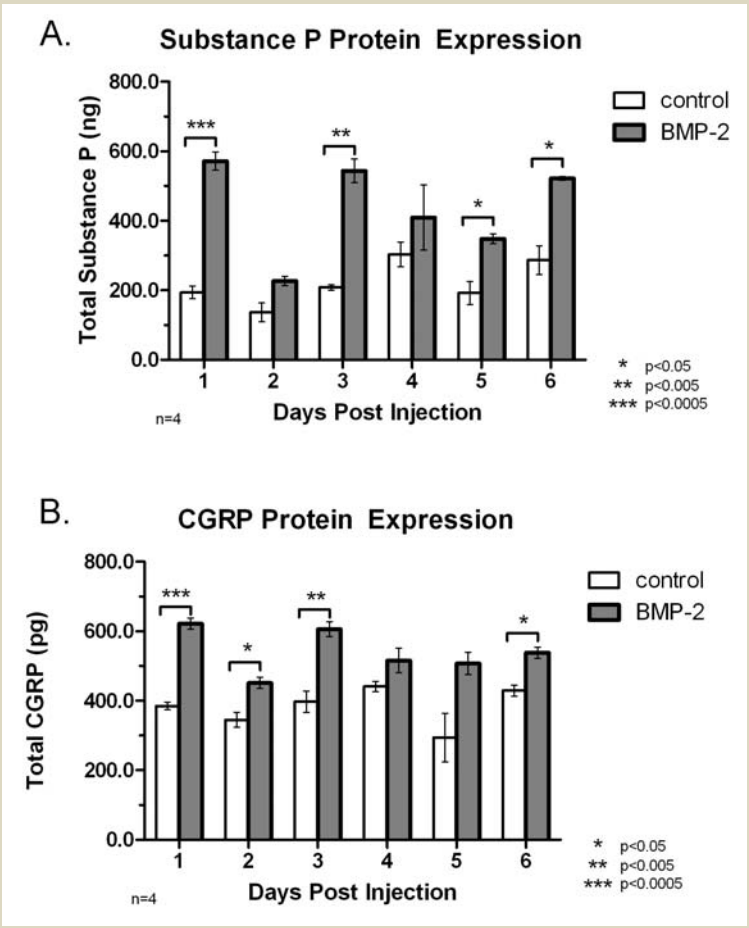

Figure 6: Quantitation of substance P and CGRP protein by ELISA. Soft tissues, which encompass the site of new bone formation, were isolated at daily intervals from animals receiving either AdBMP2 (BMP2) or Adempty (control) transduced cells, and protein extracts were generated. **A.)** Substance P total protein was quantified and statistically significant changes between the groups, as denoted by an asterisk, determined using a standard t-test; n=4. **B.)** CGRP total protein was quantified and statistically significant changes between the groups, as denoted by an asterisk, determined using a standard t-test; n=4. * denotes statistical significance.

with a post-hoc Bonferroni test for comparison between time points, verified a significant drop in SP and CGRP between days 1 and 2 ($p \leq 0.005$). This was followed by a significant rise between days 2 and 3 ($p \leq 0.005$). The data suggests that BMP2 induced a substantial and immediate release of these proteins, which was attenuated, but then continued for the remainder of endochondral bone formation, through the appearance of mineralized bone (Figure 6).

Tissues were next immunostained for the presence of SP and CGRP and analyzed to determine if the expression of these factors was associated with nerves throughout the entire hind limb, or limited to the region of new bone formation. Figure 7 shows representative images of the expression of SP and CGRP within the tissues isolated 4 days after receiving either AdBMP2 or Adempty transduced cells. By day 4 of HO, delivery cells are no longer found within the tissues, and the control appears as normal muscle (Figure 7D). However, there is a nidus of cartilage forming in tissues undergoing HO (Figure 7A). Figure 2 shows the positive expression of SP (green) or CGRP (red) in these tissues. As seen in figure 7, panels D-F, we observed a small amount of positive expression associated with a mature nerve structure within control tissues, but expression was not found within the muscle itself. In contrast, in tissue receiving BMP2, expression was co-localized with the region undergoing cartilage formation and was limited to this region. This suggests that the expression of these factors is associated with BMP2, as predicted, and the continued expression of these factors was localized to new cartilage and bone formation.

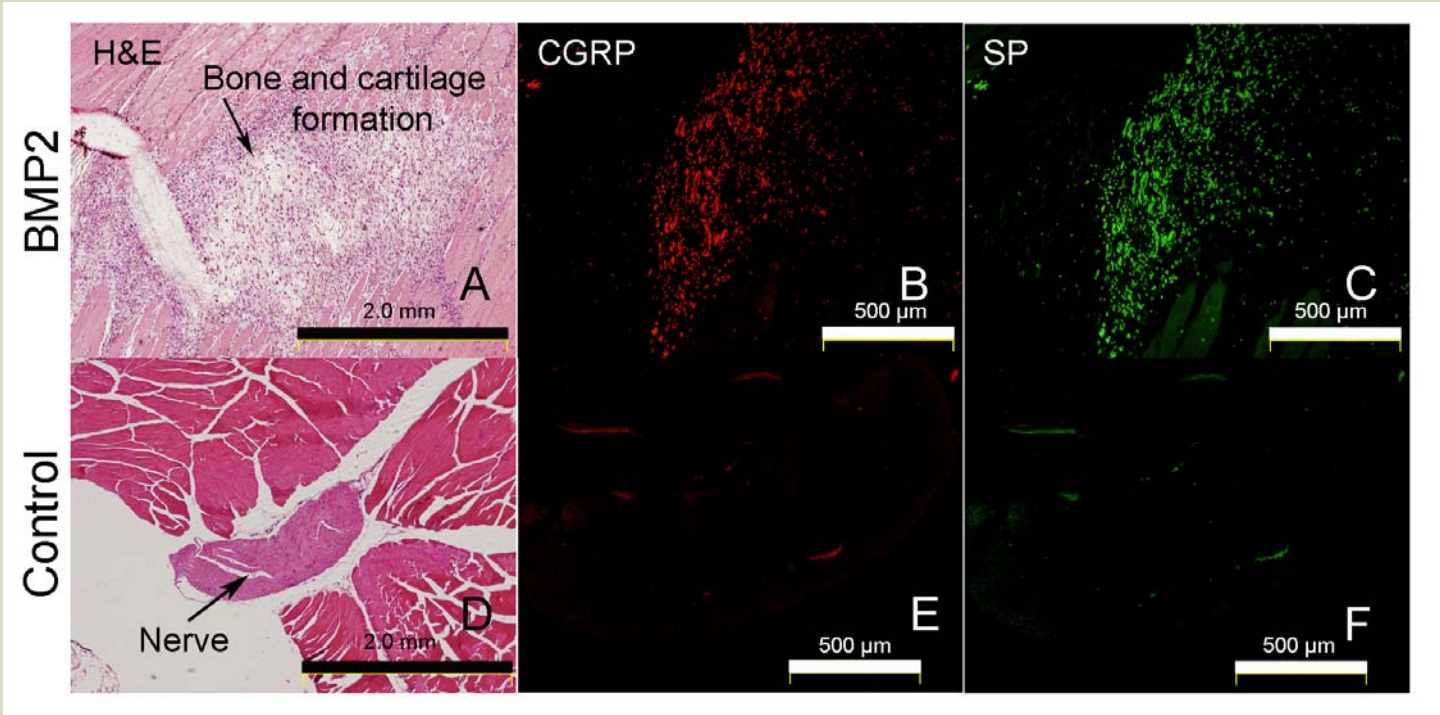

Figure 7: Photomicrographs of substance P and CGRP protein expression in tissues isolated four days after induction of HO. Tissues receiving cells transduced with AdBMP2 (BMP2) or Adempty cassette (control) were isolated four days after induction and immunostained with antibodies against substance P and CGRP. Expression of these factors was found to co-localize with the area of newly forming bone, but was minimal in tissues receiving the Adempty cassette transduced cells. Hematoxylin and eosin stained serial sections, adjacent to the section used for immunostaining four days after receiving **(A)** AdBMP2 transduced cells or **(D)** Adempty cassette transduced cells. Positive staining in the region of new bone (**B and C**) or nerve (**E and F**) for CGRP (B and E; red color) or substance P (C and F; green color).

The induction of neuroinflammatory mediators occurs through activation of sensory neurons by localized stimulus, or, in this case, secretion of BMP2. To determine if induction of neuroinflammation is contributing to HO, bone formation was quantified in animals that lacked TRPV1 ($TRVP1^{-/-}$), resulting in a functional loss of activity of sensory neurons. These $TRVP1^{-/-}$ animals lack a functional cationic channel on peripheral, sensory nerve terminals, which regulate neurogenic inflammation. We quantified the changes in SP and CGRP protein expression within tissues isolated from these knockout animals, and observed a significant suppression compared to the wild type counterpart, although we did observe a slight increase in their expression upon delivery of BMP2.

HO was induced in both TRVP1$^{-/-}$ and wild type mice (n=7), and, after 10 days, the resultant bone formation was quantified through micro-computed tomography (μCT). Figure 8A shows a representative three dimensional reconstruction of the bone formation. Heterotopic bone volume within TRVP1$^{-/-}$ mice was inhibited significantly ($p \leq 0.05$), as compared to wild type mice (Figure 8B).

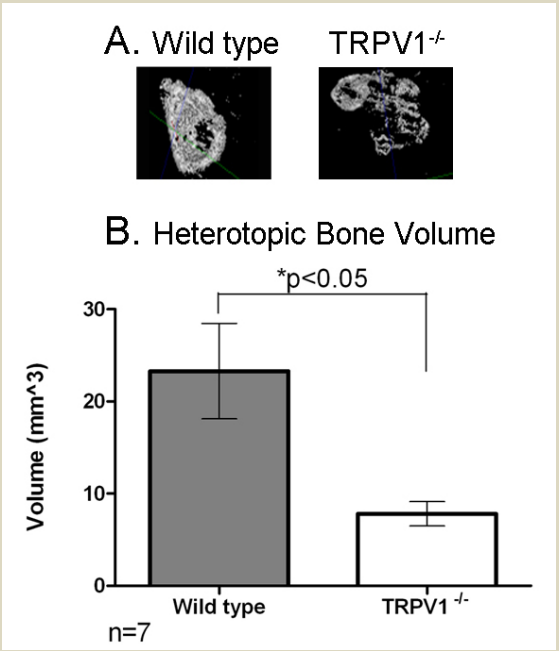

Figure 8: Microcomputational analysis of heterotopic ossification ten days after induction with AdBMP2 transduced cells, in C57/BL6, wild type or TRVP1$^{-/-}$ mice. **(A)** Three dimensional reconstructions of representative samples for each group. **(B)** Quantitation of bone volume and statistically significant changes between the groups was determined using a one-way analysis of variance; n=7. * denotes statistical significance.

for the release of SP and CGRP within the tissues, suggesting mast cells may be recruited after release of these factors.

Since mast cells are known to migrate throughout the tissues, co-localization with specific tissue structures was also noted. As seen in figure 9C, mast cells appeared to be scattered throughout the control tissues. However, within the tissues receiving AdBMP2 transduced cells, mast cells associated only with the nerves (figure 9B), in tissues isolated 2 days after induction of bone formation. As bone formation continues, the mast cells within the tissues receiving BMP2 continue to be localized within the nerve itself; however, a subset also appear within the vessel structures (data not shown). We did not see mast cells localizing within the nerve structures in control tissues at any time point.

The reduction of HO when there is a lack of functional TRVP1 signaling suggests that this pathway may be functionally important to the process of HO. The next step in neuroinflammatory signaling involves recruitment of mast cells and their resultant degranulation, for the release of key enzymes involved in processing proteins essential for inflammatory signaling and recruitment. To determine whether mast cells were recruited to the site of new bone formation, muscle tissues from the hind limbs of wild type mice injected with AdBMP2 or Adempty transduced cells were isolated at daily intervals and then serially sectioned in entirety for quantification. There appears to be a trend toward more mast cells within the tissues undergoing HO, as compared to the control tissues (figure 9A). However, only day 2 shows a statistically significant increase in the number of mast cells. It is intriguing that we observed the most significant difference at these early stages, since this appears to parallel our findings

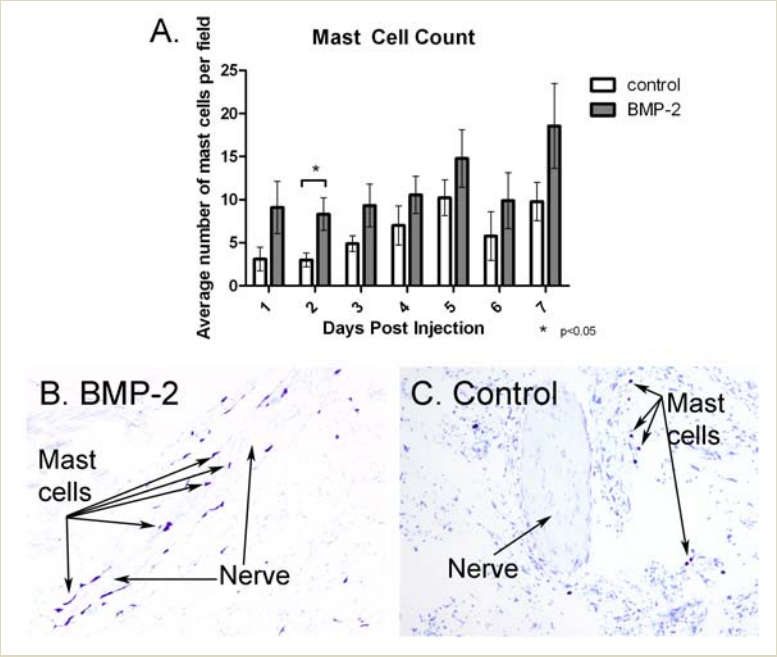

Figure 9: Quantitation of mast cells in tissues surrounding the area of new bone formation. Tissue sections were stained with the mast cell stain, toluidine blue. Photomicrographs of random fields (5 per section) were taken at 10X magnification, for every fifth slide, throughout the entire hindlimb. Each field equals 5.2mm^2. **(A)** Quantification of the average number of mast cells within the tissues at daily intervals after induction of HO. Statistically significant changes were determined using a standard t-test; n=3 biological replicates. Seven slides were analyzed per tissue, and 5 fields per slide (35 images quantified per sample/time point). * denotes statistical significance. **(B)** Representative photomicrographs of tissues isolated two days after receiving AdBMP2 (BMP2) or Adempty (control) transduced cells, stained with toluidine blue. Positive cells are highlighted with arrows.

Mast cell degranulation leads to the release of degradative enzymes, such as tryptase and chymase. These enzymes are known to degrade or process other proteins, leading to their activation. Many of the enzymes are involved in tissue remodeling, including the nerve structure itself. To determine if mast cell degranulation could be a factor in heterotopic ossification, animals were pretreated with the drug sodium cromoglycate (cromolyn), which has been shown to prevent mast cell degranulation. Following the pretreatment with either cromolyn or a vehicle control (PBS), HO was induced and the resultant bone formation quantified 10 days later. Figure 10A shows representative images of three dimensional reconstructions of the resultant HO formation after cromolyn or control, PBS treatment. As can be seen in figure 10B, quantification of bone volume of the HO shows a significant ($p \leq 0.05$) decrease in animals after cromolyn treatment. The observed decrease in HO formation after cromolyn treatment was similar to that observed in the TRVP1 null mice, thus supporting the idea that suppression of this pathway inhibits HO.

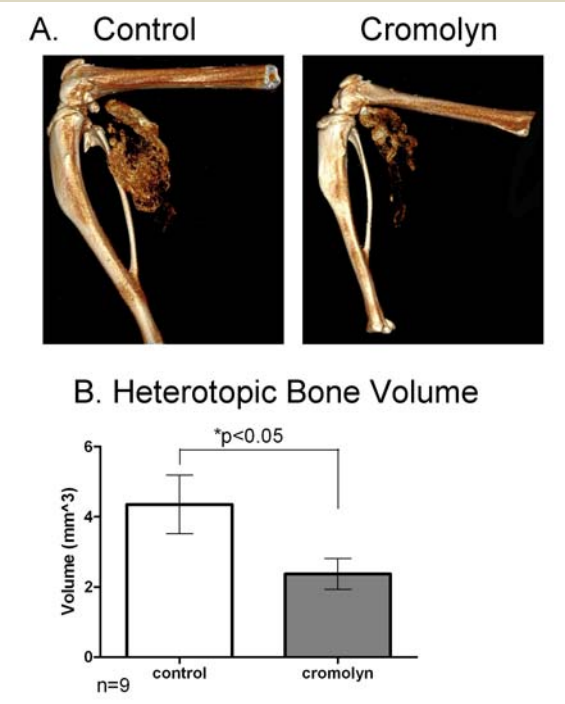

Figure 10: Microcomputational analysis of heterotopic ossification ten days after induction with AdBMP2 transduced cells, in mice pre-treated with either cromolyn or vehicle control (PBS). **(A)** Three dimensional reconstructions of representative samples for each group. **(B)** Quantitation of bone volume and statistically significant changes between the groups was determined using a one-way analysis of variance; n=9. * denotes statistical significance.

The data collectively suggests a molecular model in which sensory neurons signal to induce neuro-inflammatory mediator expression and mast cell migration and degranulation, which ultimately facilitate HO. Since others have shown that progenitors reside within the nerve sheath [30] and can expand upon nerve remodeling after injury, we analyzed the nerves isolated in hind limb tissues from cromolyn or vehicle treated animals after induction of HO. We hypothesized cromolyn treatment would block nerve remodeling, and thus, the ultimate release of progenitors perhaps residing within the nerve. The tissues were immunostained for expression of a variety of stem cell markers, and, intriguingly, we observed changes in the subset of markers related to pluripotency. Figure 11A shows representative photomicrographs of tissues immunostained for expression of Nanog and Krüppel-like family of transcription factor 4 (Klf4) within the tissues isolated two days after induction of HO. As seen in 11A, in animals that received cromolyn, cells positive for these factors were observed throughout the nerve (Fig 11A; c,d), as demonstrated by neurofilament staining (Fig 11A; b,f). However, in tissues isolated from animals that received vehicle, these markers were significantly reduced, to completely absent throughout the nerve (Fig 11A; g, h). We observed $nanog^+$ and $Klf4^+$ cells within tissues isolated from wild type animals undergoing HO, but such cells are rare and are often not co-localizing with the nerve. Both these markers have been implicated in maintenance of the pluripotential phenotype observed in embryonic stem (ES) cells, with Klf4 actually enhancing the expression of the nanog gene in ES cells. Interestingly, the osteoblast specific transcription factor osterix was also found associated with the nerve sheath (figure 11B). Osterix expression was observed in the nerve by co-staining with the neural marker neurofilament (figure 11B; g, h, i), in tissues isolated 2 days after BMP2 induction, in the presence of cromolyn. These osterix positive cells also appeared to co-localize with a portion of the primitive stem cell factors, suggesting that a subset of the cells may be undergoing differentiation (Figure 11B, panels a-f).

This work demonstrates the ability of the secreted BMP2 to induce neuro-inflammation which leads to

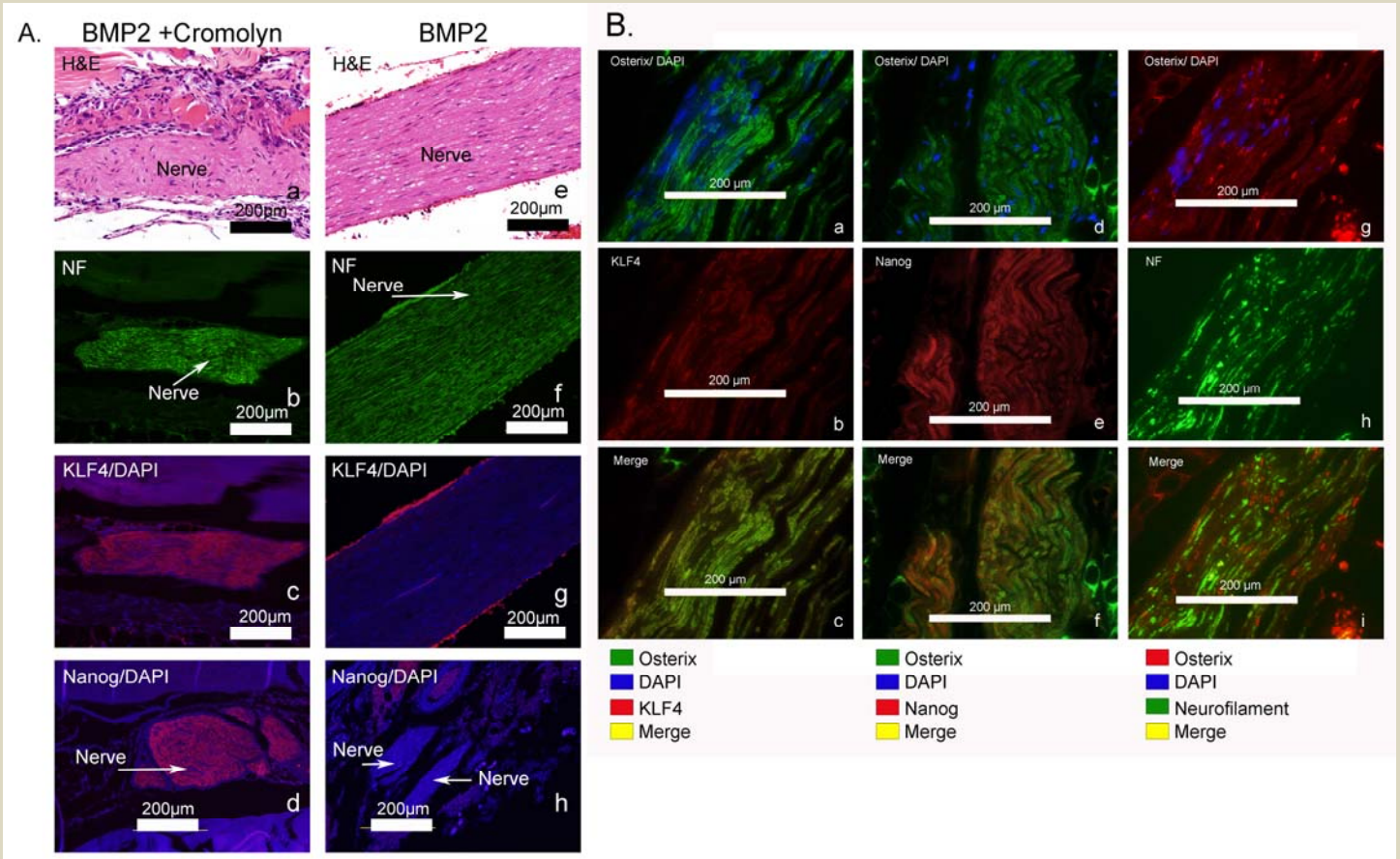

Figure 11. Peripheral nerves contain primitive stem cell markers and osterix after BMP2 induction in the presence of cromolyn. **A.** Photomicrographs of tissues isolated two days after induction of HO. Tissues from animals receiving cells transduced with AdBMP2 and pre-treated with either cromolyn (a-d) or vehicle control (e-h) were isolated two days after induction, and immunostained with antibodies against stem cell markers, Klf4 and Nanog. Expression of these factors was found to co-localize to nerves residing within the area of new bone formation. Nerves were identified by hematoxylin and eosin staining of a serial section adjacent to the immunostainned tissues (**a** and **e**) and by neurofilament (NF) staining (**b** and **f**; green color). Positive staining for Klf4 (**c**; red color) or Nanog (**d**; red color) was observed throughout the nerves in tissues isolated from animals receiving cromolyn at 2 days after induction. In comparison, the nerves in animals receiving vehicle control appeared to lack positive staining for either Klf 4 (**g**; red color) or nanog (**h**; red color). **B.** Photomicrographs of osterix expression within tissues isolated two days after BMP2 induction in the presence of cromolyn. Images of osterix expression (**g**; osterix red color, DAPI blue color) associated with the nerve (**h**; neurofilament, NF, green color). **i**, osterix and NF, is a merger of g and h. Images of the expression of **a, d** osterix (green, DAPI blue) and **b**, Klf4 (red) or **e**, nanog (red). **c**, osterix and Klf4, is a merger of a and b. **f**, osterix and nanog is a merger of d and e.

the release of factors and recruitment of mast cells for the remodeling of the local peripheral nerves. This appears to be critical to the process of de novo bone formation, in that inhibition of this process, led to a significant reduction in bone formation. Further, we demonstrate the appearance of osterix positive cells within the remodeling nerve. These cells appear to be expanding and trafficking off the nerve towards the region where new bone will be established. Interestingly, these cells appear 2-3 days prior to the appearance of any bone, suggesting that this marker may be expressed for other reasons than to induce the osteogenic phenotype or that these new osteoprogenitors may reside within the vessel structures until oxygen tension is restored through cartilage removal and vascular invasion (Shafer *et al,* 2007; Olmsted-Davis *et al,* 2007, and Fouletier-Dilling *et al*, 2010).

From the experiments in this aim, we have determined that the level of BMP2 in our experiments most likely is maximum and thus longer expression times do not appear to extend the reaction. However, the ability to target the exact placement of the material can not only increase the bone volume (Olabisi *et al*, 2010), but that it increased the area of responder tissues. Further we have identified one of the first direct immediate responsed in to BMP2 within the localized tissues is from the peripheral nerve. This activation of the nerve is

essential to bone formation, and results in the migration of several cell populations from the nerve. One of these populations appears to be a pre-osteoblastic population that migrates towards the vessel structures, where it is housed until 2-3 days later when vessels infitrate the hypertrophic condrocytes, and deposit the osteoblasts (Salisbury *et al*, J Cell Biochem). Further our data suggests that these nerves associated stem cells, are also the precursor for brown adipose, an essential tissue for vascularization, and patterning of the newly forming cartilage (Olmsted-Davis et al, 2007). Therefore we propose that perhaps the early expression of osterix 2-3 days prior to the appearance of bone may be a mechanism to suppress the adipose phenotype in a sub-population of the cells. Further, the population of these stem cells which do not immediately associate with the vessels, but rather migrate into the adipose and muscle tissues, expresses the beta-adrenergic receptor 3 sub type, which has been shown to generate brown adipose. Isolation of these cells shows the co-expression of uncoupling protein 1 within these cells, and RNA studies of the tissues shows a significant increase in both mRNA's during this time, suggesting that activation of sensory neurons by BMP2, may launch of a cascade of events, that activates sympathetic neurons, presumably through release of serotonin by mast cells and platelets. Further, immediate recruitment of platelets to the local site, leads to the release of monocyte chemoattractant factors which can recruit myeloid cells necessary for vascular invasion, and bone formation. Therefore we have identified a pathway for BMP2 induced bone formation which requires both nerve and inflammatory signaling to occur, and demonstrated that ablation of this pathway will ultimately ablate bone formation and healing.

Task 2: To design an optimal hydrogel material that will rapidly promote endochondral bone formation and be capable of removal through bone remodeling processes. In addition to BMP2 transduced cells, we propose to include peptides essential to the recruitment and migration of osteoprogenitors for bone and cartilage. Selective protease sites will also be introduced into the hydrogel to allow for osteoclast selective degradation during bone remodeling. We propose to do this by incorporation of calcium into the material and inclusion of cathepsin K protease cleavage sites into the material. Inclusion of these factors in the hydrogel will provide a mechanism for removal of the hydrogel once bone has formed by using the normal bone remodeling process.

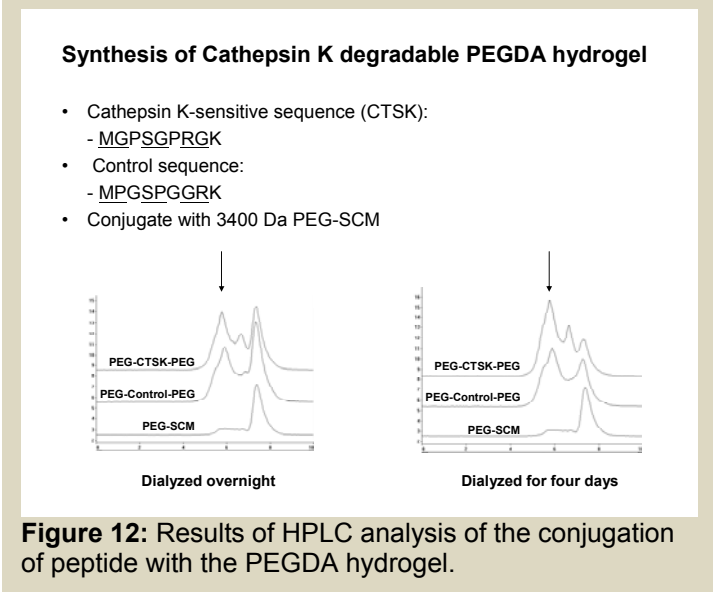

Figure 12: Results of HPLC analysis of the conjugation of peptide with the PEGDA hydrogel.

a. Optimize and develop a hydrogel that can be specifically degraded by osteoclasts.

(Months 0-24)

We have synthesized the peptide MGPSGPRG (Gowen et a;1999) using a 431A solid-phase peptide synthesizer (Applied Biosystems, Foster City, CA). In order to make degradable PEG, we start with PEG-DA-SMC (succinimidyl carbonate). The PEG-SMC is conjugated with our peptide in order to get PEG-PEPTIDE-PEG. So, we expect to obtain three peaks representing the completely conjugated product: PEG-PEPIDE-PEG, incompletely conjugated product: PEG-PEPTIDE and unconjugated product: PEG-SMC (Figure 12).

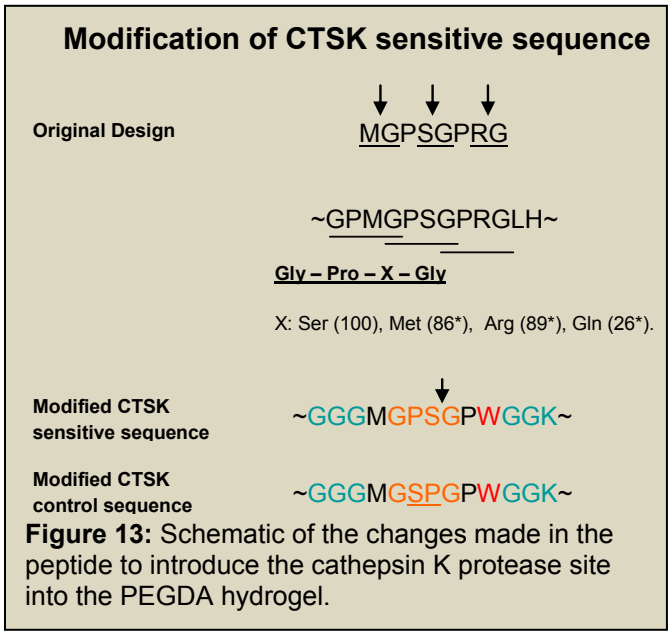

Figure 13: Schematic of the changes made in the peptide to introduce the cathepsin K protease site into the PEGDA hydrogel.

We have run GPC tests on it and the results indicate that there is still unconjugated PEG, ie: we have PEG-Peptide or free PEG in the preparations. We have tried changing the ratio of peptide to PEG, changing the length of conjugation time, increasing the pore size of the dialysis membrane and changing the

length we dialyze the conjugation products. These have led to a higher concentration of PEG-PEPTIDE-PEG as indicated by the GPC results (Figure 13). We have cathepsin K (Calbiochem; Cathepsin K, His•Tag®, Human, Recombinant, *E. coli*). Degradation tests have found that the material did not degrade as expected. Analysis of the materials suggested that the protease site may be too confined to actually bind enzyme for digestion, thus, the protease site was redesigned to have a longer amino acid sequence linker to allow for better digestion. Thus the modified peptide sequence is GGGMGPSGPWGGK, see figure 13.

We next examined the ability of the cathepsin K sensitive hydrogels to degrade in the presence of the enzyme. The hydrogels with the cathepsin K sensitive peptide GGGMGPSGPWGGK were designed to carry a cathepsin K sensitive cleavage site between serine and proline. Proteinase K was used as a positive control. While the gel degrades, the peptide that was incorporated into the hydrogel structure will be cleaved by enzymes and gradually release into solution. The degradation profiles of GPSG hydrogels were measured by monitoring the concentration change of tryptophan in solution at UV absorbance of 280 nm. Crosslinkable GPSG hydrogels were polymerized in microcuvettes and incubated with enzyme solutions. After equilibrium swelling in TBS overnight, hydrogels were treated with different enzymes to evaluate the degradation profiles (Figure 14). After incubation with different enzyme solutions for 24 hours, hydrogels in cathepsin K and proteinase K solutions has similar degradation profiles, both indicating a rapid tryptophan concentration increase within the first hour and reaching about 80% release of total tryptophan at 24 hours. No degradation was observed when hydrogels were incubated in TBS buffer, NaOAc buffer, and plasmin. Hydrogels incubated in nonspecific collagenase I and collagenase III solutions also released 40% of incorporated tryptophan after a 24 hour incubation (figure 7). ***This work has recently been accepted for publication in Journal Biomaterials Research (Chih-Wei Hsu, Ronke M. Olabisi, Elizabeth A. Olmsted-Davis, Alan R. Davis, Jennifer L. West Cathepsin-K sensitive poly(ethylene Glycol) hydrogels for degradation in response to bone formation. This subaim is completed.***

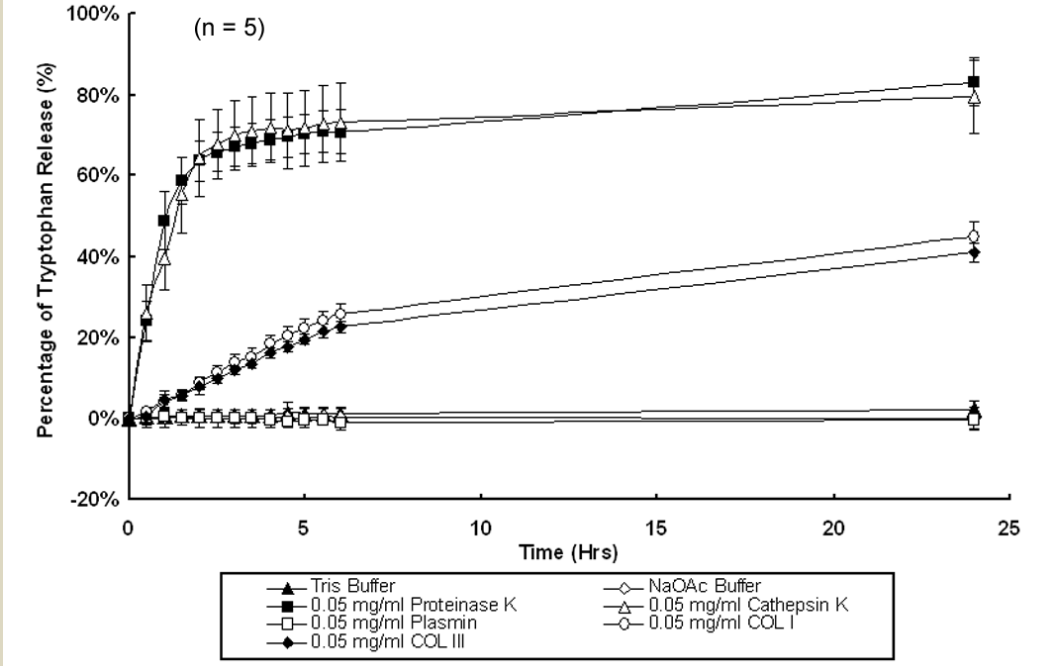

Figure 14: Degradation profiles of cathepsin K-sensitive GPSG hydrogels. Hydrogel droplets (3 µl) were polymerized in each micro-cuvette and swelled overnight with 250 µl of TBS buffer. Each hydrogel was incubated in buffer or enzyme solution at 0.05 mg/ml at 37^{O}C. UV absorbance at 280 nm was measured over 24 hours to monitor tryptophan release corresponding to the degradation of the GPSP hydrogels.

b. Engineer cellular binding sights within the hydrogel to determine if this improves, cell viability of the transduced cells, and in turn BMP2 expression, and to tentatively enhance the migration of mesenchmyal stem cells to the sight of bone formation. **(Months 0-24)**

We have introduced RGD binding sites within and throughout the hydrogel to enhance binding of the osteoclasts (see above section) as well as other cell migration. This has been very effective in allowing cells to bind to the material, during bone formation. Additionally, inclusion of the RGD binding sites within the material has appeared to greatly enhance cell viability, allowing for the cells to remain viable. However, the most optimal improvement for BMP2 expression and cell viability has come from altering the structures to be microspheres, rather than larger beads (Bikram *et al*). Comparison of the BMP2 secretion from larger hydrogel structures to the microbead structures, showed a significant improvement. Figure 15 shows the BMP2

expression from larger bead structures, in comparison to the cells which were not encapsulated (Plated cells).

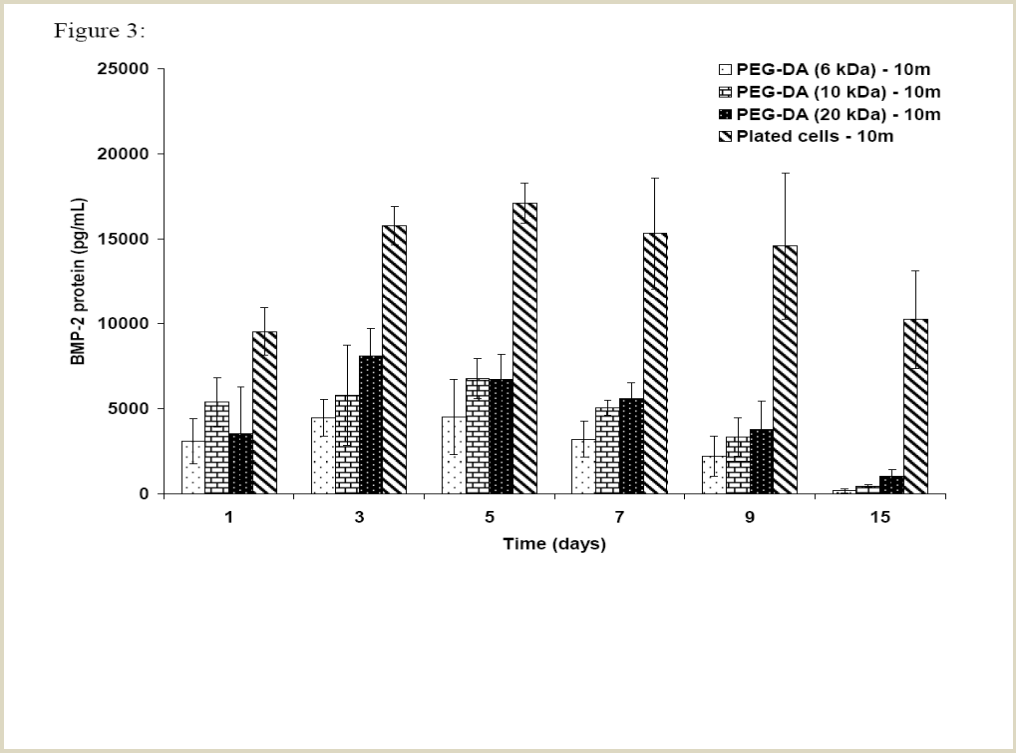

Figure 15: Western blot analysis for the detection of secreted BMP-2 protein. (a) Human recombinant BMP2 (lane 1), conditioned medium from PEG-DA (10 kDa) hydrogels only (lane 2), conditioned medium from 10 million MRC-5 cells encapsulated within PEGDA (10 kDa) hydrogels (lanes 3 and 4), conditioned medium from 10 million transduced fibroblasts control (lanes 5–8), human recombinant BMP-2 (lane 9), conditioned medium containing secreted BMP-2 protein from 10 million transduced fibroblasts encapsulated within PEG-DA (10 kDa) hydrogels (lanes 10–17). (b) Alkaline phosphatase activity in W20-17 cells without the addition of conditioned medium (W20-17) and after addition of conditioned media from PEG-DA (10 kDa) hydrogels with 10 million transduced fibroblasts and control plated transduced fibroblasts (Days 1–15). Data reported as mean ± SD, n = 5.

As seen in Figure 15, the BMP2 expression is reduced by 50% in culture supernatants isolated from the encapsulated cells within the bead structures, as compared to the plated cells.

We chose to next re-engineer the encapsulated structures, into microspheres, which hold between 0-100 cells. As seen in figure 16, within the microspheres, live cells converted the non-fluorescent calcein AM into green fluorescent calcein while ethidium homodimer freely passed through the permeable membranes of dead cells to bind the DNA and fluoresce red. Encapsulated cells showed high viability 95 ± 0.5 %, suggesting that they were not adversely affected by the microencapsulation process.

We also compared the level of BMP2 in culture supernatant taken from both cells directly plated and cells encapsulated in microspheres. BMP2 activity was quantified by measuring alkaline phosphatase (AP) activity in W20-17 cells exposed for 72 hours to the culture supernatants from AdBMP2-transduced cells directly plated or encapsulated in microspheres was significantly elevated over control cells but there was no difference between these groups, indicating the BMP-2 released is functionally active (Figure 17A). A 9 day time course of BMP-2 levels in culture supernatant was quantified by ELISA to be approximately 17,500 pg/ml and 15,000 pg/ml for directly plated and microencapsulated cells, respectively (Figure 17B). No BMP-2 was detected in either culture supernatant from AdEmpty cassette-transduced cells, or control cells. The results suggest that the smaller structures, may allow

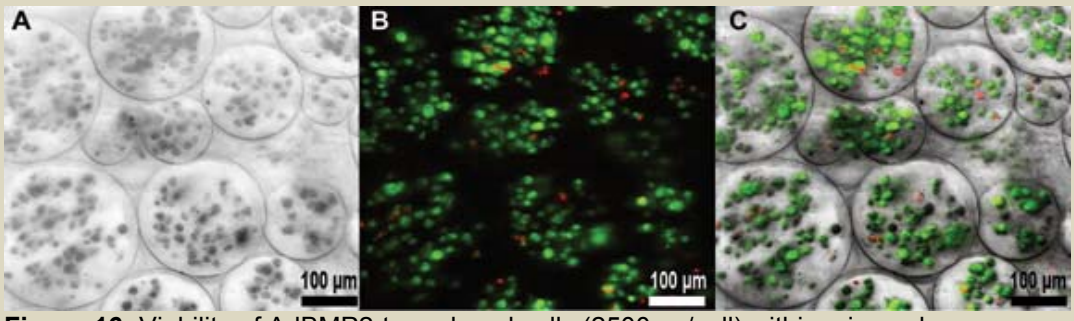

Figure 16: Viability of AdBMP2-transduced cells (2500 vp/cell) within microspheres was assessed at day 7 using a LIVE/DEAD® Viability/Cytotoxicity Kit for mammalian cells (Invitrogen, Molecular Probes, Eugene, OR). **A.** Minimum intensity projection of a differential interference contrast (DIC) Z-stack. **B.** Maximum intensity projection of fluorescent Z-stack merge of red and green channels. The red channel was thresholded to eliminate diffuse virus staining. Dead cells appear red and live cells appear green. **C.** Overlay of panels A and B. Living cells accounted for 95.08% ± 0.47% of total cells encapsulated.

for both greater cell viability and diffusion of BMP2.

MicroCT analysis of bone formation showed a significantly greater volume of heterotopic ossification in tissues receiving microspheres (Figure 18A, C) than those receiving directly injected cells (Figure 18B, D). Statistical power to detect differences between volumes formed in these groups was 72.5%. Cross-sectional microCT analysis of the newly formed bone revealed a similar architecture between the groups. Heterotopic bone formed by both the microencapsulated cells and directly injected cells had a pattern of dense bone surrounding a hollow interior (Figures 18C and D); however the circumference of bone within the directly injected cells was significantly smaller. Microencapsulated AdBMP2-transduced cells produced approximately twice the bone volume of unencapsulated cells (Figure 19B). Despite the volumetric increase, the bone tissue mineral content was statistically similar between these groups, although trending towards an elevation in samples that received the microspheres (Figure 19A). This corresponds with the change in tissue mineral density of the new bone surrounding the microspheres (Figure 19C). The newly formed bone appears to be slightly less dense, leading to the overall similarity in mass between the two groups. Statistical power to detect differences between bone densities in these groups was 76.7%.

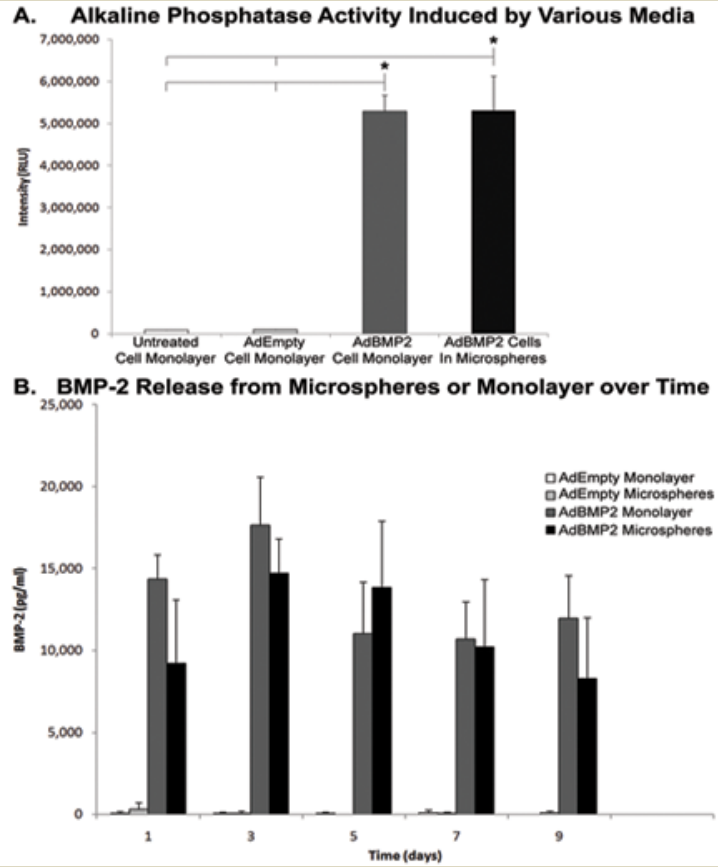

Figure 17: Comparison of BMP-2 expression, secretion and activity after PEGDA encapsulation. **A.** BMP-2 protein in culture supernatant taken from AdBMP2- or AdEmpty cassette-transduced cells (25000 vp/cell) (monolayer), or those encapsulated in PEGDA microspheres was quantified by sampling every other day for 9 days and evaluated using an ELISA. **B.** Alkaline phosphatase activity in W20-17 cells after addition of conditioned media from AdBMP2- or AdEmpty cassette-transduced cells (25000 vp/cell) (monolayer), or AdBMP2-transduced cells encapsulated in PEGDA microspheres. As a negative control, we also included culture supernatant from untransduced cells. Alkaline phosphatase activity is depicted as the average relative chemiluminescence units (RLU), where n=3. Error bars represent means ± SD for n=3. A Student t-Test was applied to demonstrate significance. AdBMP2-transduced monolayer and microsphere groups had significantly greater alkaline phosphatase activity and BMP-2 concentration levels ($p < 0.05$) when compared against other groups, but no differences when compared to each other. In other words, microencapsulation had no effect on BMP-2 release and function.

From histological analysis, both groups had significant new bone formation within the muscle (Figure 20). In tissues that had received the direct injection of AdBMP2-transduced cells, there was a small compact piece of bone forming a ring-like structure encircling what appears to be blood and tentative stroma, and just exterior to this structure was significant adipose (Figure 20A). A similar structure was observed in tissues that had received microspheres (Figure 20B). Since the microspheres did not degrade, they appear histologically as gaps or holes within the matrix (Figure 20B). Thus, despite the presence of nondegradable microspheres, both structures were patterned to have a denser bone structure with a bone marrow-like cavity on the interior. **This work has been published in *Olabisi, R. et al, Tissue Engineering Part A. Dec 2010, 16(12):3727-36.* *This sub-aim is completed.***

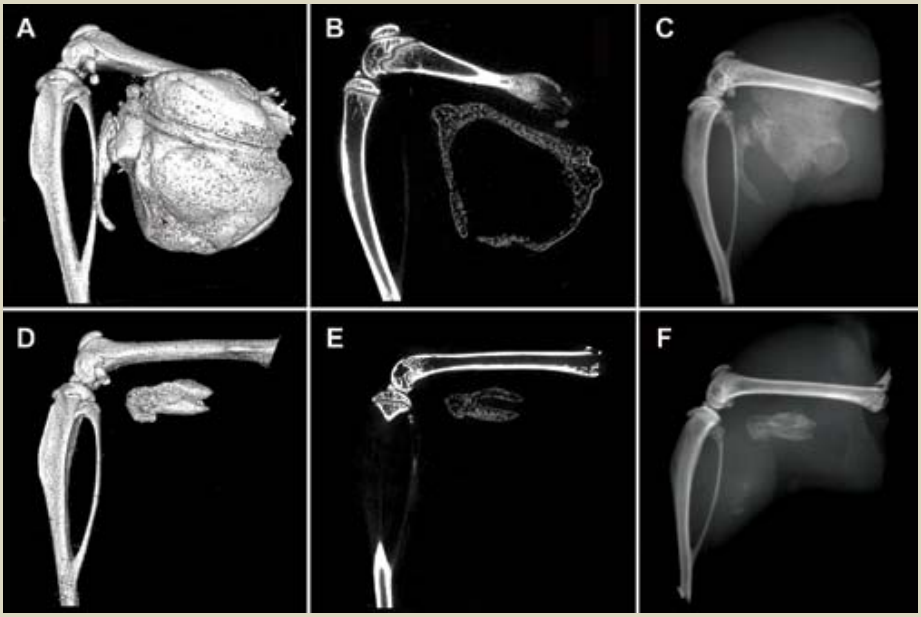

Figure 18: Micro computational analysis of the resultant heterotopic bone formation. Left images (**A, D**) are 3D surface renderings of the resultant heterotopic bone, while middle images (**B, E**) are cross-sectional slices through the new bone. Right images (C, F) show corresponding radiograms. Panels A - F show the resultant mineralization of the muscle tissues after injection of AdBMP2-transduced cells (2500 vp/cell) encapsulated into PEGDA microspheres (**A - C**) or direct injection of unencapsulated AdBMP2-transduced cells (**D - F**). Both have a denser rim of bone, with a hollow interior structure, suggesting that the biomaterial did not alter bone patterning.

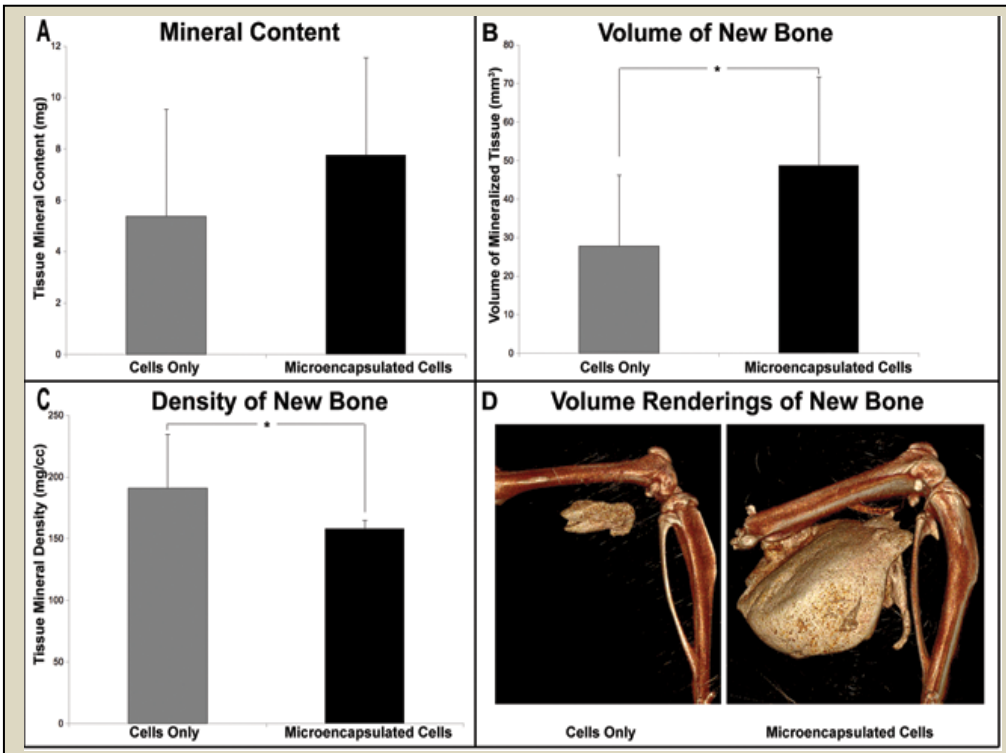

Figure 19: Quantification of the heterotopic ossification using microcomputational analysis. Cells were transduced with AdBMP2 and either directly injected or encapsulated into microspheres prior to injection, and the resultant heterotopic bone was analyzed two weeks later. Tissue parameters: **A.** bone tissue mineral content, **B.** bone volume of mineralized tissue, and **C.** bone tissue mineral density were calculated for the newly formed bone (n=6 per group). The means and standard deviations for each group were calculated and compared using a one-way analysis of variance. Results indicate that mineral content is statistically equivalent (p=0.2) between the groups, whereas the AdBMP2-transduced cells in microspheres had a significantly greater volume (p=0.038) than the AdBMP2-transduced cells directly injected. Alternatively, the bone tissue mineral density was significantly denser for the group receiving the cells directly as compared to those in microspheres (p=0.029). Panel **D.** shows a 3D volume rendering of new bone formed in cell only and microencapsulated cell groups, respectively.

c. Test addition of proteins that may enhance the BMP2 bone inductive response, such as VEGF-A or –D and compare enhancement of bone formation. (Months 24-36)

We have recently published the significant elevation in these VEGF proteins after expression of BMP2 in the local tissues (Fouletier-Dilling, et.al. J Bone Miner Res. 25(5):1147-56. 2010 PMID: 19839764). From this work, additional delivery of VEGFs does not enhance the reaction, or new vessel formation, most likely because this is maximally activated. ***Therefore this subaim is completed.***

d. Test these gels in vitro. (Months 12-36)

We next tested the degradable hydrogel to determine if it could be selectively degraded by osteoclasts. Raw 264.7 cells were differentiated in culture medium containing 30 ng/ml RANKL for 4 days. Cells collected through gradient centrifugation and placed in culture where they were enzymatically stained for tartrate acid phosphatase activity (TRAP). Multinucleated cells in the culture appeared to stain positive for TRAP suggesting that they had undergone osteoclast differentiation. The majority of cells at the bottom fraction of the gradient contained the TRAP+ dRAW 264.7 osteoclasts were then used for hydrogel degradation studies. To demonstrate the ability of the cells to

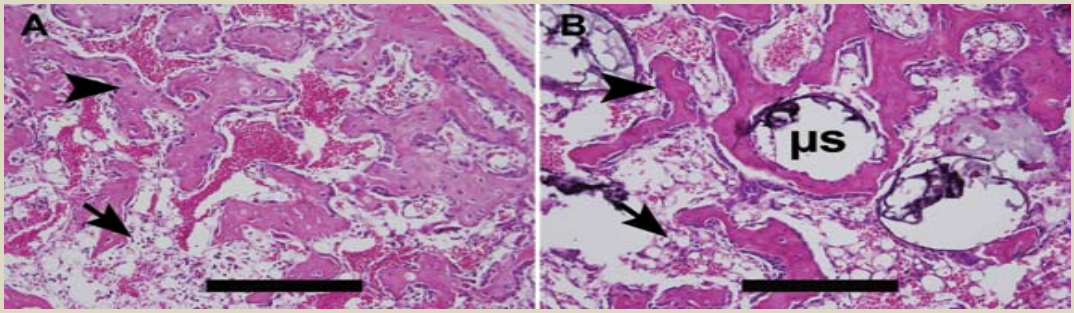

Figure 20: Photomicrographs of heterotopic ossification. Hematoxylin and eosin stains of new bone formation by: **A.** directly injected and **B.** microsphere (μs) encapsulated cells. Both groups show small compact pieces of bone (arrowheads) forming ring-like structures, encircling what appears to be blood and tentative stroma in the inner region, with significant adipose (arrows) just exterior to the new bone. Scale bars are 500 μm.

both adhere to the hydrogel material so a normal substrate for growth, as well as have the selectivity in degradation, we next plated both primary osteoblasts and the TRAP+ dRAW264.7 osteoclasts onto GPSG hydrogel sheets containing the RGD binding sites which were preformed, to provide a smooth surface to ensure they do not possess imperfections other than those introduced by degradation from the cell populations.

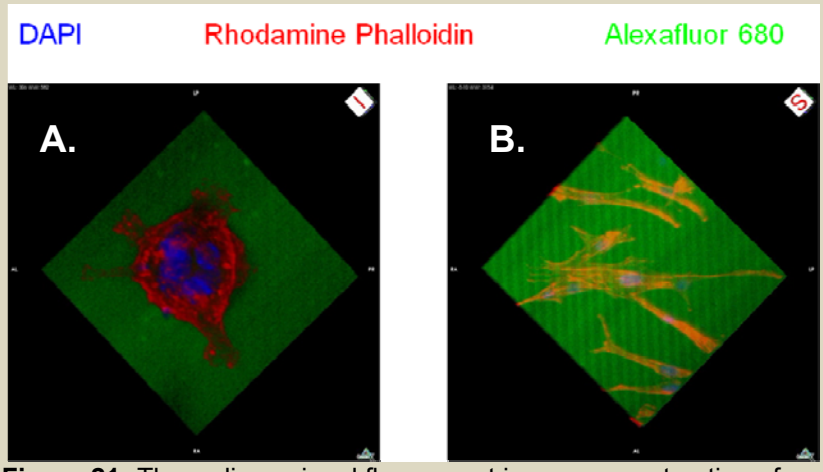

Figure 21: Three-dimensional fluorescent image reconstruction of an active osteoclast on the GPSG hydrogel surface. The GPSG hydrogel was labeled with Alexafluor 680 fluorophore (green), which is conjugated with the acryloyl-PEG-RGDS and incorporated into the hydrogel by photo-polymerization. The cells were fixed and permeabilized before staining the nuclei with DAPI (blue) and F-actin by rhodamine phalloidin (red) 48 hours after seeding. (A) Composed z-stack images of the osteoclast on hydrogel. (B) Composed z-stack images of osteoblasts on hydrogel. Osteoblasts did not appear to leave any pits.

As can be seen in figure 21, both cell types readily adhered to the material, and formed normal cell structures observed in tissue culture. The degradable or GPSG hydrogels possessing Alexafluor 680 (green color) were fixed and stained with DAPI (blue color) for nuclei and rhodamine (red color) phalloidin for F-actin in the cytoplasm. As can be seen in figure 21 and 22, observed on hydrogel surface were actual resorption pits generated by RAW264.7 osteoclasts which were absent on the GPSG hydrogels which had been seeded with osteoblasts. Hydrogels-osteoclasts interactions were examined under confocal microscopy at higher magnification. Multinuclear and polarized cells RAW264.7 osteoclasts were identified on the hydrogel surface, (Figure 22A). A sealing ring of F-actin and multiple nuclei were clearly observed (Figure 22B). On the hydrogel surface where the osteoclast was located, a decrease in the fluorescent signal was observed (Figure 22C). The z-stack images were then examined closely by three-dimensional reconstructions using a volume rendering method. Figure 22D is the side view, showing the osteoclast attached to the hydrogel. From the three-dimensional perspective of the image from the top (Figure 22E) and bottom (Figure 22F) of the hydrogel, the loss in fluorescent signal of the hydrogel reveals a hole in the hydrogel through which the cell can be seen. This signal loss is indicative of activity by the differentiated RAW264.7 osteoclasts, degrading the underlying hydrogel and creating a pit, resulting in the fluorescent intensity loss. No signal loss was observed on the gels seeded with dMC3T3-E1 cells. Therefore it appears that the osteoclasts may be selectively able to remodel the hydrogel material as predicted. ***This work has recently been accepted for publication in Journal Biomaterials Research (Chih-Wei Hsu, Ronke M. Olabisi, Elizabeth A. Olmsted-Davis, Alan R. Davis, Jennifer L. West Cathepsin-K sensitive poly(ethylene Glycol) hydrogels for degradation in response to bone formation.*** ***This subaim is completed.***

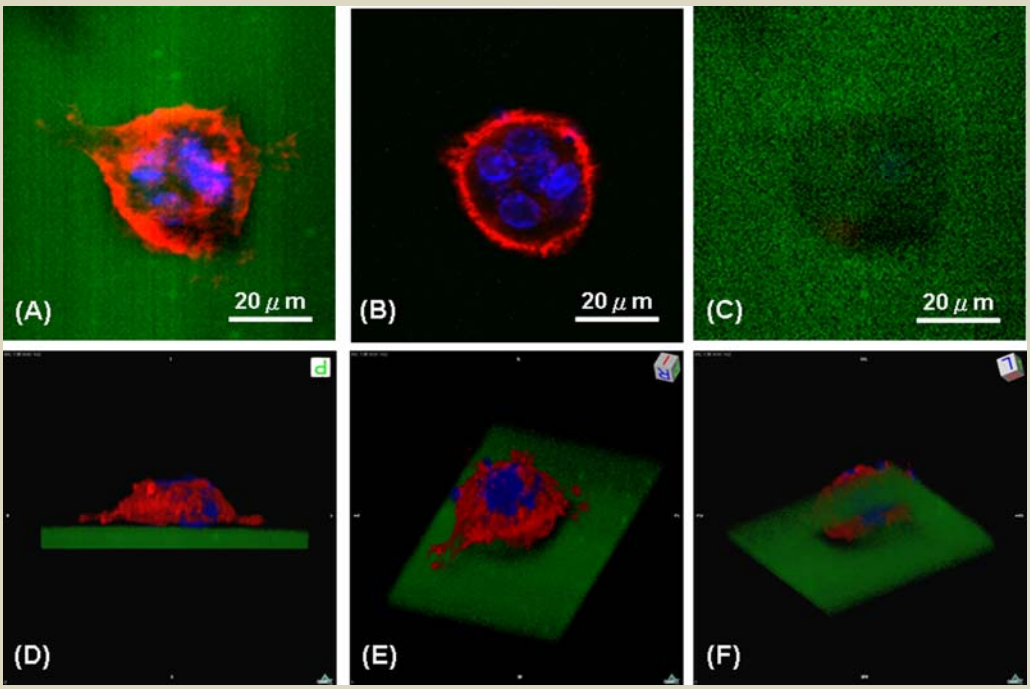

Figure 22: Three-dimensional fluorescent image reconstruction of an active osteoclast on the GPSG hydrogel surface. The GPSG hydrogel was labeled with Alexafluor 680 fluorophore (green), which is conjugated with the acryloyl-PEG-RGDS and incorporated into the hydrogel by photo-polymerization. The cells were fixed and permeabilized before staining the nuclei with DAPI (blue) and F-actin by rhodamine phalloidin (red) 48 hours after seeding. (A) Composed z-stack images of the osteoclast and hydrogel. (B) Sealing ring and multiple nuclei of the osteoclast. (C) GPSG hydrogel with fluorescent signal lost at middle. Z-stack Images were reconstructed using the volume renderings algorithm and presented from (D) side view, (E) orthogonal view from above, and (F) from bottom. The resorption site is located underneath the osteoclast, which was can be observed in the loss of the fluorescent intensity of Alexafluor 680. The resorption pit on the hydrogel surface can be clearly seen from different angles, suggesting that the GPSG hydrogel has been degraded by cathepsin K secreted by osteoclasts.

Test these gels in vivo. ***(Months 36-48)*** We next tested the material *in vivo* to determine if we observed degradation, and replacement of the microspheres with bone. We injected the microspheres, and then approximately 3 weeks after injection harvested the tissues, processed, and sectioned through the newly formed heterotopic ossification to detect the microspheres. Figure 23 shows a representative photomicrograph of a hematoxylin and eosin stained section of heterotopic bone and bone marrow. Intact microspheres can be detected within this section; however, there are also microspheres within the maturing bone that appear to be degrading. Further, the yellow rectangle encompasses a region which appears to be newly formed heterotopic bone, in the shape of a microsphere, suggesting that the removal of that material may be complete at this time. We are currently completing this *in vivo* analysis for

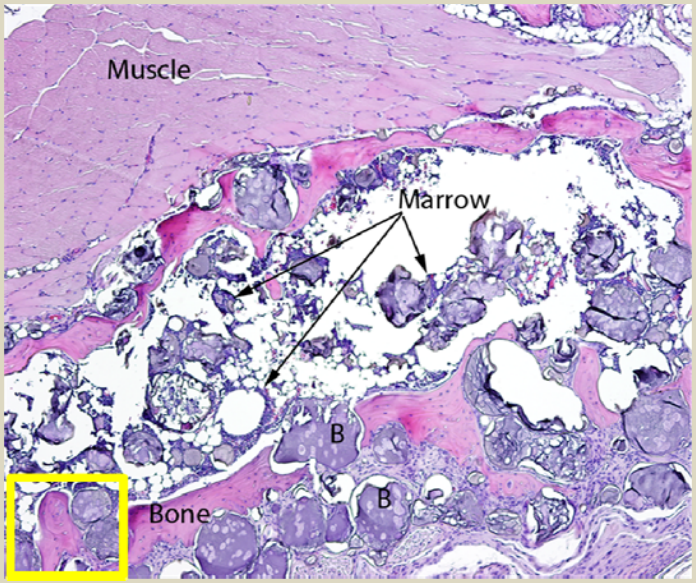

Figure 23: Photomicrograph of a hematoxylin and eosin stained tissue section depicting the degradation of the microbeads *in vivo*.

Task 3: To achieve rapid bone formation by percutaneous injection of the encapsulated Ad5F35BMP2 transduced human bone marrow mesenchymal stem cells (hBM-MSCs) into the adjacent musculature of athymic rats in a model of nonunion.

a.Obtain approvals through the DOD institutional review board for approval to work with the human mesenchymal stem cells. (Months 0-12) We have approval to use human mesenchymal stem cells either encapsulated or unencapsulated for in two models for critical size defects in both Athymic as well as Wistar rats. The two models are the fibula which is fused to the tibia and therefore does not require additional fixation, as well as the femur model, which involves external fixation to maintain the defect and non-union. We have generated both rat MSCs and human MSCs but have found that skin fibroblasts appear to be

more stable within the hydrogels and data shown below suggests that they are more reliable for achieving rapid bone formation *in vivo*. ***This subaim is completed***.

b. Once the gels have been modified to offer optimal properties for bone formation and removal, we will test these in a rat model of a critical-size defect. We will demonstrate the ability to induce bone healing in the presence of tetracycline. (Months 24-40) We have completed the studies with the hydrogel and found that the optimal structure is to produce microbeads or microspheres which encapsulate 0-100 cells and provide high cell viability long term, and comparable BMP2 expression *in vitro* to those which are not encapsulated (See task 1 section).

Figure 24:

c. Analyze the modified injectable hydrogel for optimal volume, in vivo crosslinking, design, selective degradation, and inflammatory reaction using both live animal imaging and histology. (Months 24-48) We have previously determined that crosslinking of the hydrogel *in vivo* leads to reduction in BMP2 expression from the cells, and also provides for a shape which is suboptimal for inducing bone formation. We have determined that the optimal structure for inducing targeted bone formation is to pre-form the hydrogel encapsulated cells into microspheres or beads, which are injectable, and can be placed within the tissue defect to recruit cells for *de novo* bone formation. We have induced heterotopic bone using these microspheres, and found that we observe normal looking bone, and no apparent inflammatory reaction to the hydrogel or allogenic cells, and thus bone formation can occur rapidly at the targeted site. *(See above sections).* ***This work has been published in Olabisi, R. et al, Tissue Engineering Part A. Dec 2010, 16(12):3727-36. This sub-aim is completed.***

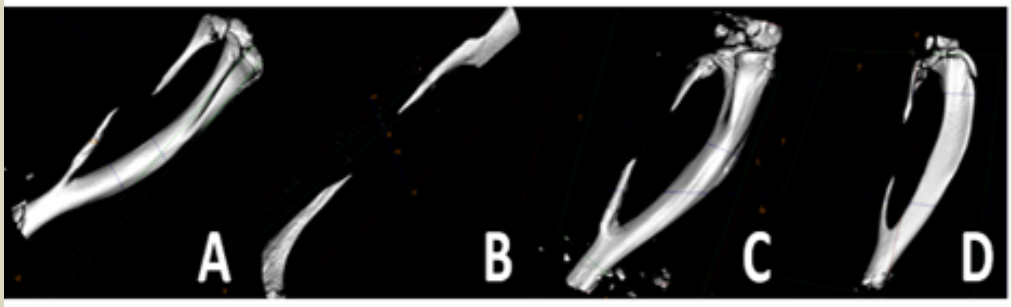

Figure 25: Representative three dimensional reconstructions of rat fibulas through microcomputational analysis. Varying sizes of defects (1 mm - 10 mm) were surgically introduced into rat fibulas and two weeks later analyzed for the presence of bone repair. The results depicted show an approximately 10 mm defect independent of the original defect size **(A)** 1 mm, **(B)** 2 mm, **(C)** 5 mm and **(D)** 10 mm.

d. Bone healing will be tested both biomechanically as well as radiologically using microCT to confirm the fusion. (Months 40-48) Approvals have been obtained from Baylor College of Medcine and more recently from the Department of Defense for all the animal models. We next established a model of critical size defects in rat long bone. Varying sizes of bone were removed from the rat fibula starting with a simple fracture (1mm), and systematically increasing in one millimeter increments to a maximum of 10 mm. The rat fibula was selected over other potential bones because unlike in humans, in rodents this bone is uniquely fused to the adjacent tibia. Therefore, a critical defect can readily be introduced without need for additional fixation. After 2 weeks bone healing was radiologically evaluated using microcomputational tomography (μCT). Surprisingly, in all cases 1 mm, 2 mm, 5 mm, and 10 mm defects (Fig. 25A-D, respectively) we observed a similar size defect of approximately 10 mm or the maximum size introduced into the bone, and the bone ends appeared to be pointed, suggesting that the bone was undergoing significant resorption.

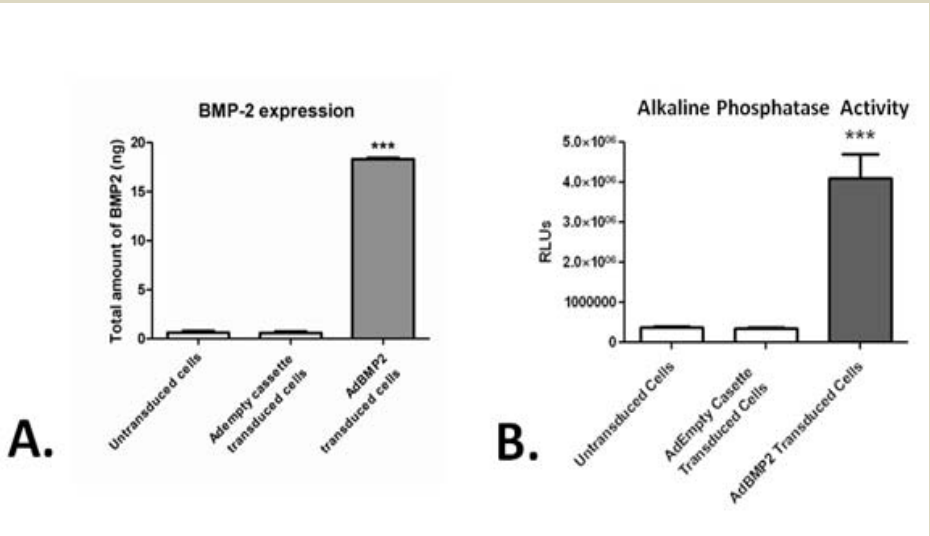

Figure 26: Quantification of BMP2 protein and activity from adenovirus transduced cells. **A.** BMP2 activity in culture supernatant collected 72 hours after transduction with AdBMP2- or AdEmpty cassette-transduced cells (25000vp/cell) was quantified using an ELISA. BMP2 protein is represented as total protein produced by 5 x 10^6 cells. Error bars represent means ± SD for n=5. A student t-Test was applied to demonstrate significance. **B.** Alkaline phosphatase activity in W20-17 cells after addition of conditioned media from AdBMP2- or AdEmpty cassette-transduced cells (25000 vp/cell). To demonstrate endogenous levels of alkaline phosphatase we included the cells alone. Alkaline phosphatase activity is depicted as the average relative chemiluminescence units (RLU), where n=3. Error bars represent means ± SD for n=3. A Student t-Test was applied to demonstrate significance.

We next defined the dose of AdBMP2 transduced cells required to provide optimal healing of the bone defect. Fibroblasts were transduced with AdBMP2 at 2500vp/cell and BMP2 protein as well as activity was quantified 72 hours later. Total BMP2 protein within the culture supernatant was approximately 18.6 nanograms per 1 x 10^6 cells (Fig 26A). Cells transduced with AdEmpty, as well as untransduced cells, did not produce BMP2. Interestingly, a standard dose of recombinant BMP2 protein used to induce bone formation in a rat critical size defect was approximately 12 ugs. Since 5 x 10^6 BMP2-producing cells is adequate to heal the bone completely (Fig. 27A), and we have determined that the transduced cells are present at a maximum of 5 days. This means that a maximum of 93 ng is sufficient to completely heal the bone in this model. This is 130

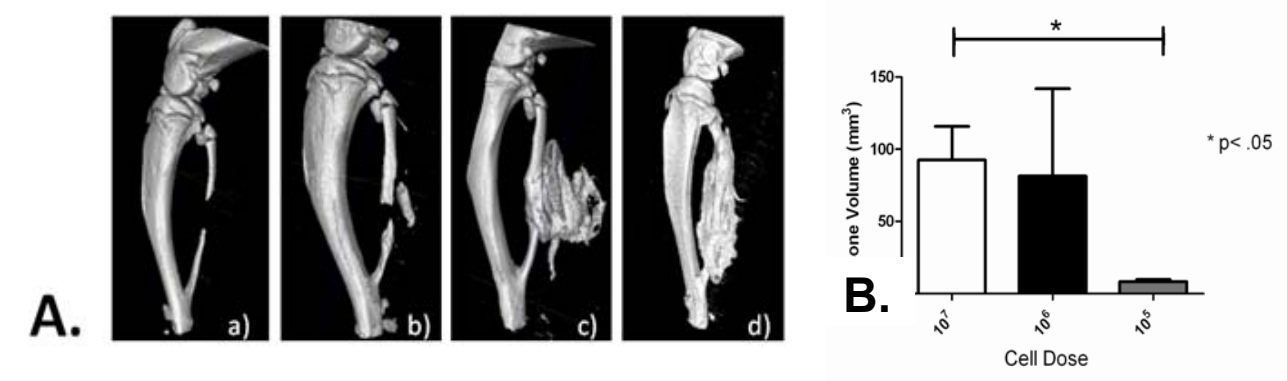

Figure 27: Resultant bone formation from the introduction of adenovirus transduced cells into the defect site. **A.** Representative three dimensional surface renderings obtained from micro computational analysis of the resultant bone repair two weeks after introduction of critical size defect in the rat fibula and delivery of varying numbers of AdBMP2 transduced cells; **(a)** 5 x 10^4 cells **(b)** 5 x 10^5 **(c)** 5 x 10^6 **(d)** 5 x 10^7. **B.** Quantification of the bone repair using microcomputational analysis. Bone volume of the newly forming bone as depicted in Figure 3A, was calculated for each cell dose (n=5 per group). The means and standard deviations for each group were calculated and compared using a one-way analysis of variance.

times less than the amount of protein used in other rat defect studies with recombinant BMP2 suggesting that the prolonged local generation of BMP2 is critical to success due to the short half life of the protein.

Further, BMP2 protein activity, as determined by the elevation in the BMP2 responsive protein alkaline phosphatase, showed that this BMP2 being made is active (Fig. 26B). At no time did we observe either BMP2 activity or protein in culture supernatant isolated from the AdEmpty cassette cells or cells alone. Various numbers of the AdBMP2 transduced cells were next injected simultaneously with the introduction of a 3 mm bone defect in the fibula. The cells were injected into the void region, and surrounding muscle tissues of the rats (n=5), and potential bone formation allowed to progress for two weeks. Representative images of the

resulting new bone are shown in Figure 27. As seen in Figure 27A, the new bone formation varied drastically with cell numbers. At no time did we observe bone formation or healing in the samples receiving 5 x 10^4 cells, suggesting that there is a threshold amount of BMP2 required for inducing bone formation. Alternatively, there was no statistical difference between the two highest cell numbers or doses (27B), indicating that there is a maximum bone formation response that can be achieved with this system. No bone formation was observed in with the 5 x 10^4 cell dose, whereas there is a significant 10 fold change in bone volume between the 5 x 10^5 and 5 x 10^7 cell doses. There was significant difference between the highest doses 5 x 10^6 and 5 x 10^7 suggesting that there this may be a maximum response to BMP2. For that reason, we used this dose for all subsequent experiments.

We next determined the ability of the therapy to heal the critical size defect over 12 weeks. Figure 28 shows there is substantial bone formation at 2 weeks using this dose of cells, which appears to quickly resorb and by 4 weeks the new bone more closely resembles the fibula that it is replacing. However, as seen in the cross sectional μCT (Fig. 28F) new bone appears to be immature in nature. Although it spans the defect and is contiguous with the skeletal bone, it has not remodeled to have contiguous cortices, which suggests that this may not be well integrated at this stage. Alternatively, by 6-12 weeks a cortical bone structure begins to

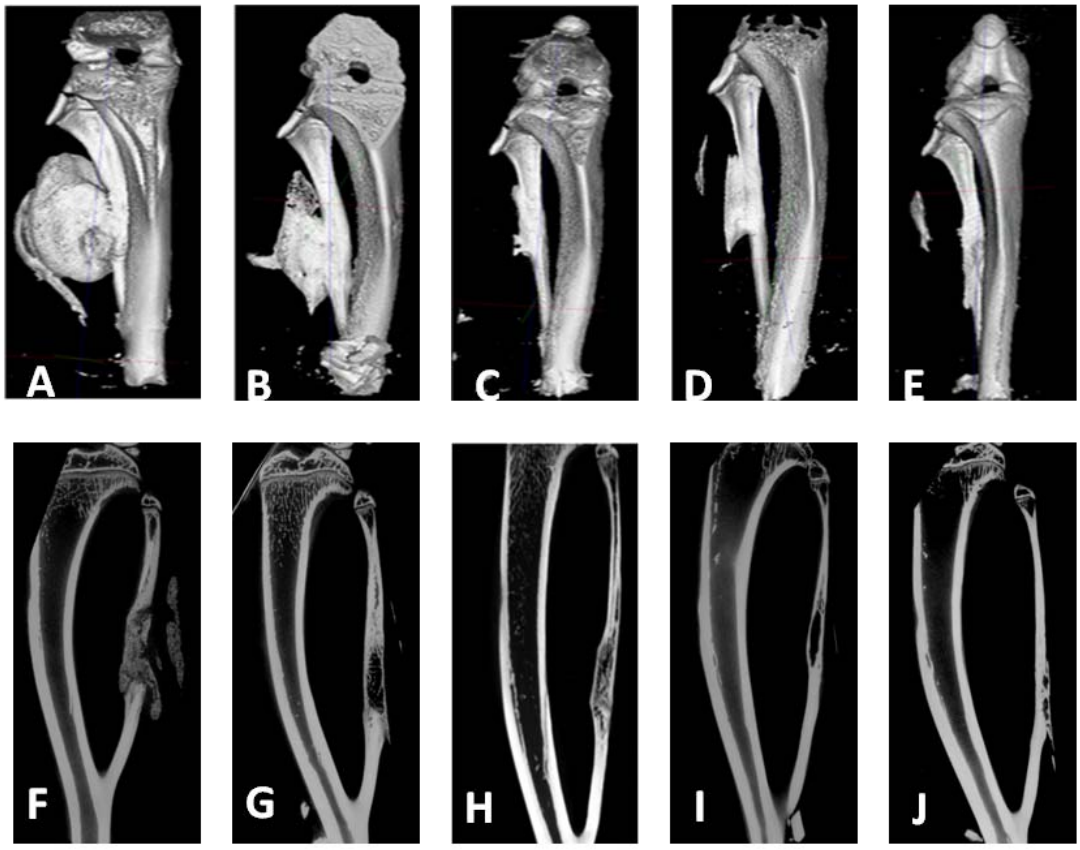

Figure 28: Micro-computational analysis of bone healing over time. Representative three dimensional surface renderings (A-E) or two dimensional reconstructions (F-J) of bone healing over time; **(A and F)** 2 weeks; **(B and G)** 4 weeks; **(C and H)** 6 weeks; **(D and I)** 9 weeks; and **(E and J)** 12 weeks after introduction of the AdBMP2 transduced cells in the fibula defect; n=9 per group.

appear in the newly formed bone (Fig. 4H-J), suggesting that the bone is being remodeled and most likely fused. Bone healing and remodeling appears to be complete by 6 weeks (Fig. 4H) with little additional remodeling occurring at weeks 9 through 12. Interestingly, there appears to be additional bone attached to the skeletal bone (Fig. 28C-E), or actual residual heterotopic ossification that has not been resorbed. Additionally, some samples appeared to have a small amount of residual heterotopic ossification which was not attached to the fibula, but remained in the muscle between fibers.

We next looked at the bone architecture by analyzing cross-sectional cuts through the bone. The architecture appeared to change dramatically over the course of bone healing. Changes in bone architecture are a component of bone remodeling and aid in determining if the new bone has truly fused to the skeletal bone. Fusion at the defect site is a critical parameter in this system, because the majority of the new bone is made *de novo*, as heterotopic ossification, and it must fuse to the skeletal bone to complete healing. At 2 weeks the new bone is found throughout the skeletal defect (Fig. 28F); however, it appears to be immature bone, which has not remodeled or integrated into the adjacent skeletal bone. This is in contrast to the adjacent skeletal bone, which has well defined cortices and a hollow bone marrow cavity. Thus although there is new bone, it does not appear to be well fused into the skeletal bone, or healed to the point such that it is one contiguous remodeled structure. However, by 6 weeks portions of the new bone appear to be remodeled with defined cortical bone and the tentative fusion site are less apparent (Fig. 28H), suggesting that the bone is integrated and almost completely healed. By 9 to 12 weeks, we observed integrated structures with the only abnormality being the additional small amounts of bone on the outer cortex (Fig. 28I-J).

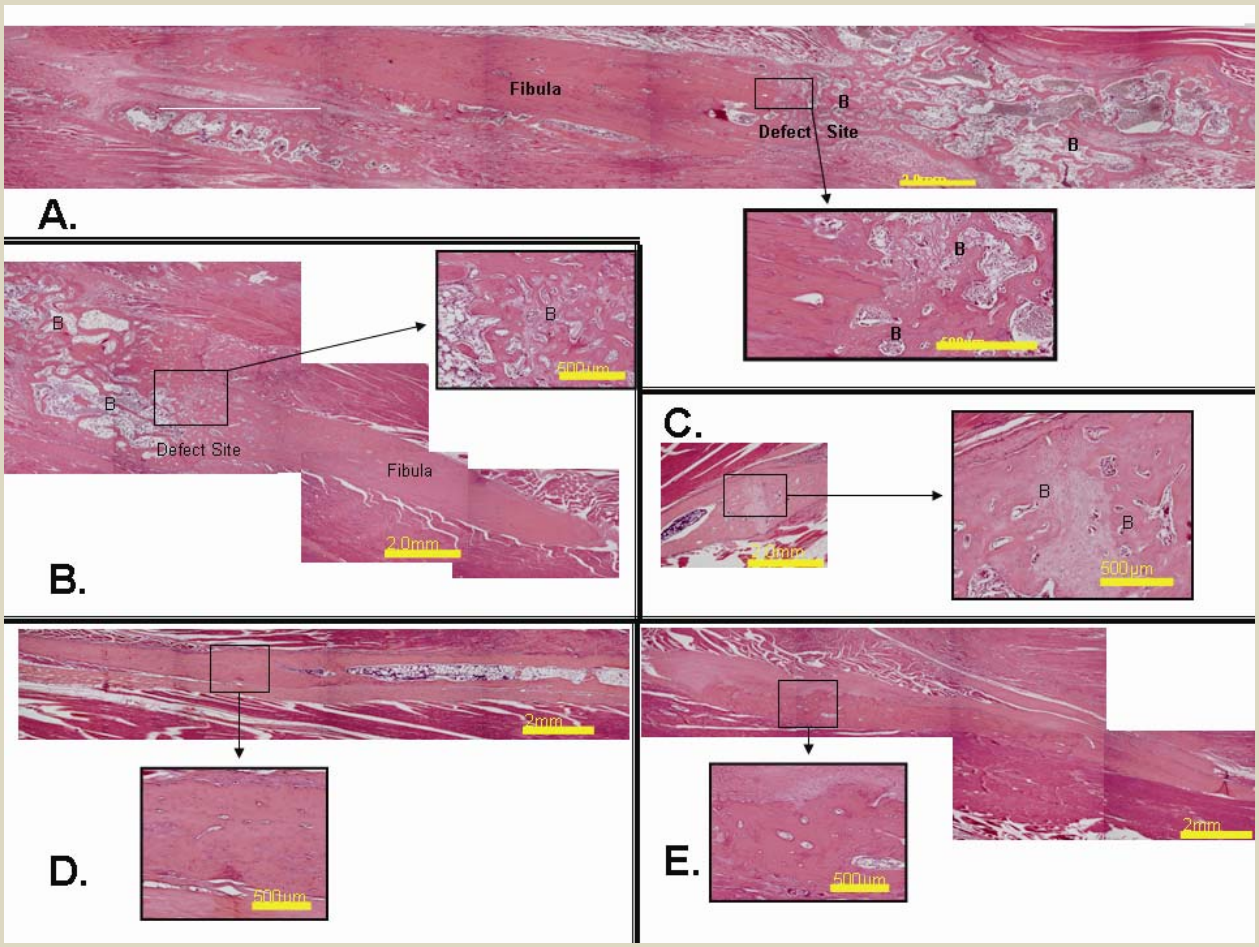

Figure 29: Representative photomicrographs of the fibula defect at various times after introduction of the AdBMP2 transduced cells. Tissues were formalin fixed decalcified, paraffin embedded and serial sectioned (5 µm) through the entire fibula region. Every fifth section was hematoxylin and eosin stained, and images taken which were representative of the defect region in particular the junction with the fibula at various times, **(A)** 2 weeks, **(B)** 4 weeks, **(C)** 6 weeks, **(D)** 9 weeks, and **(E)** 12 weeks. The appearance of bone is identified with [B].

We next examined the bone healing through histological analysis to confirm the remodeling and fusion of the newly formed bone with the skeletal bone. This requires bone remodeling to replace the woven bone and lamellar bone junction with integrated remodeled bone. Photomicrographs from representative samples of the healing fibulas show substantial immature bone that completely fills and surrounds the defect (Fig. 29). Over time however, the bone remodels considerably and new cartilage is no longer present in the tissues (Fig. 29B). By 6 weeks, the bone appears to be considerably more mature, with thicker cortical area that are contiguous with the skeletal cortical bone (Fig. 29C). Interestingly, the adjacent cortical bone appears to have a significant gap, which may represent either an area where the bone is vascularized, as evidenced by the pooling of blood

or alternatively, a defect introduced during healing (Fig. 29C). However, this defect was not observed through radiograph analysis (Fig. 29C), suggesting that it comprises a relatively small region of the new bone. It is also of interest to note that in the serial sections where this cortex appears uniform and contiguous, the adjacent cortex now appears ruffled. This indicates that although it is healing, the new shape of the bone does not exactly mimic the original fibula. At 9 and 12 weeks, there is once more additional bone on the exterior of the fibula. However, the interior cortex appears uniform and similar to the normal fibula (figure 29D and E).

We next tested the ability of the hydrogel encapsulated AdBMP2 transduced cells to induce bone healing in a critical size defect in the rat femur. In this model, we introduce a 3-5 mm critical defect within wild type rat femurs and maintained the defect through use of an external fixator (figure 30). Briefly, allogenic skin fibroblasts were transduced with AdBMP2 and 24 hours later microencapsulated through addition of a hydrogel solution (PEGDA) and mineral oil containing a photoinitiator that forms the crosslinked microsphere structures when exposed to white light. This injectable therapy is applied into the target site of a critical size defect in the rat femur. The femur was chosen because it is the largest weight-bearing bone in the body and is one of the most challenging for clinical repair. In this model, threaded pins were placed across the ends of the femur allowing for a 5 mm gap to be created in the midshaft of the bone. The pins were held in place by an external fixation device so that the rat could ambulate without either compression of the defect or significant motion. Osteoinductive microspheres are then directly injected into the femur defect (Fig. 30A). Each microsphere contains up to 100 cells and measures between 20 and 250 microns as shown in Fig.30B.

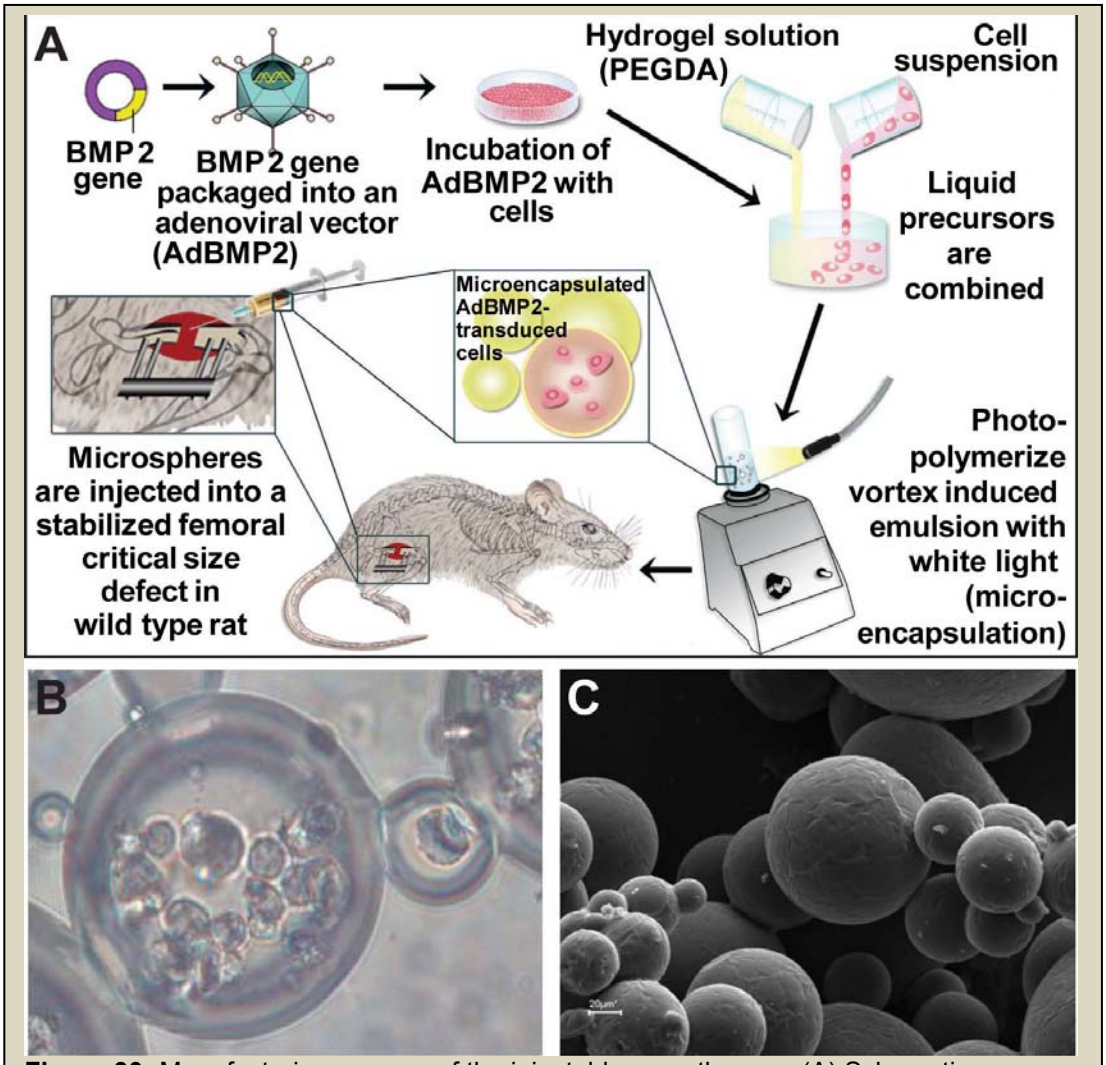

Figure 30: Manufacturing process of the injectable gene therapy. (A) Schematic depiction of the steps leading to the final osteoinductive microspheres. Briefly, allogenic skin fibroblasts were transduced with AdBMP2 (7500 vp/cell) and 24 hours later micro-encapsulated through addition of a hydrogel solution (PEGDA) and mineral oil containing a photoinitiator that forms the crosslinked microsphere structures when exposed to white light as described in Olabisi *et al,* 2010, which are easily injected into the target site. (B) Image of the osteoinductive microspheres.

We first performed dose escalation studies. No bone formation was observed in the defect in animals receiving $2x10^6$ encapsulated cells (Fig. 31A) whereas complete healing was achieved with $2x10^7$ microencapsulated cells (Fig. 31B). Culture supernatant from the AdBMP2 transduced cells that were encapsulated and injected into the rats were harvested and tested for BMP2 expression and activity. Results of this analysis suggest that these cells prior to injection were producing approximately 48 ng of BMP2 per 10^7 encapsulated cells over a 24h period (Fig. 31E). Upregulation of endogenous cellular alkaline phosphatase activity is commonly used for the assessment of osteogenic differentiation of stem cells. Alkaline phosphatase assay showed that BMP2 produced by the microspheres possesses similar bioactivity as recombinant protein (Fig. 31F).

Then, we evaluated bone formation and healing in the defect using the osteoinductive microspheres, as compared to a similar number of AdBMP2 transduced cells, which were not encapsulated in PEGDA hydrogel. When unencapsulated BMP2-producing cells were directly injected into the defect, there was no apparent bone formation and/or healing (Fig. 31C); while the same cells, when microencapsulated, were able to induce bone formation (Fig. 31D). As expected, there was no bone healing in control animals that received Adempty transduced cells microencapsulated in the PEGDA hydrogel and the defect formed a non-union fracture (data not shown).

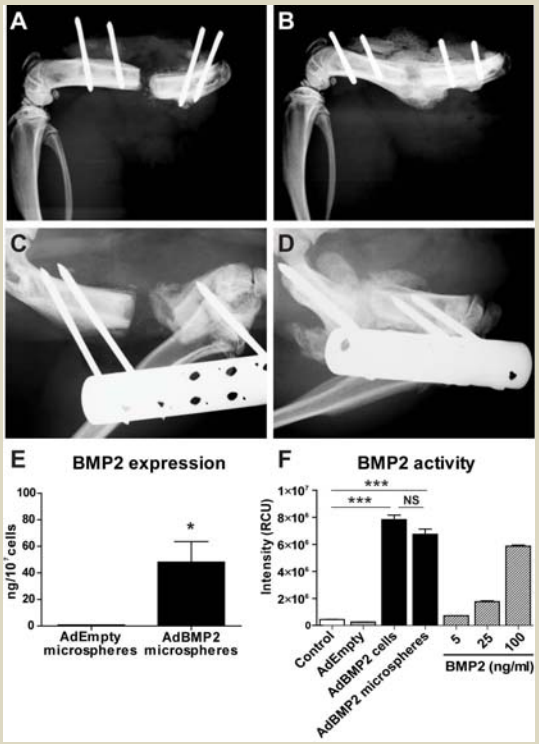

Figure 31: Osteoinductive microspheres induce bone formation in a model of femoral critical size defect in rat. (A-B) Radiographs 3 weeks after introduction of critical size defect in the rat femur and delivery of varying numbers of BMP2 expressing cells within microspheres; (A) $2x10^6$ cells and (B) $2x10^7$ cells. (C-D) Radiographs at 2 weeks post surgery and after injection of Ad5BMP2 transduced cells (C) or microencapsulated Ad5BMP2 transduced cells (D). (E) ELISA showing the amount of BMP2 protein required for response. Statistically significant changes, as denoted by an asterisk, were determined using a standard t-test; *p=0.0401 (F) Alkaline phosphatase activity in W20-17 cells after addition of conditioned media from AdBMP2- or AdEmpty cassette-transduced cells (7500 vp/cell) in monolayer or microencapsulated (microspheres). Statistically significant changes, as denoted by an asterisk, were determined using a standard t-test; ***p<0.0001; NS, p=0.0781.

The process is finite and brigding bone, once integrated, remains intact.

Consistent bone formation was observed at the targeted site at 3 weeks after surgery by X-ray (Fig. 32A) and microCT (Fig. 32F). At this time there was bone bridging the defect in 95% of the animals compared to 76% at two weeks (Fig.32K). This bridging bone did not appear to have a cortical exterior (Fig. 32F) but rather a more immature trabecular nature. However, by 6 weeks (Fig. 32B, G) the new bone appeared to have a cortical exterior and trabecular interior that bridged the defect without gaps that would suggest poor integration or non-union. This bone structure remained consistent in samples isolated at later time points 6 weeks to 12 weeks (Fig. 32B, C, D and G, H, I). The bone formation appeared finite rather than continually invasive and all rats continued to appear healthy, ambulate normally, and had no additional injuries. Neither bone formation nor spontaneous healing was observed in any of the 7 control animals (Fig. 32E, J).

Bone healing was studied longitudinally, in a subset of animals, to evaluate any changes or adverse events that may occur from result of the microspheres injection (Fig. 33). In these studies the external fixator was removed 2 weeks after surgery without disruption of the newly forming bone (Fig. 33A) and the rat was x-rayed, and then followed radiographically at 2, 4, 12, 22, 34 and 45 weeks (Fig. 33A-F). The shape of the area of new bone formation did not appear to change significantly from 2 weeks to 11 months, as seen in figure 4. However, the bone appeared to become more mineralized with time, suggesting remodeling was occurring.

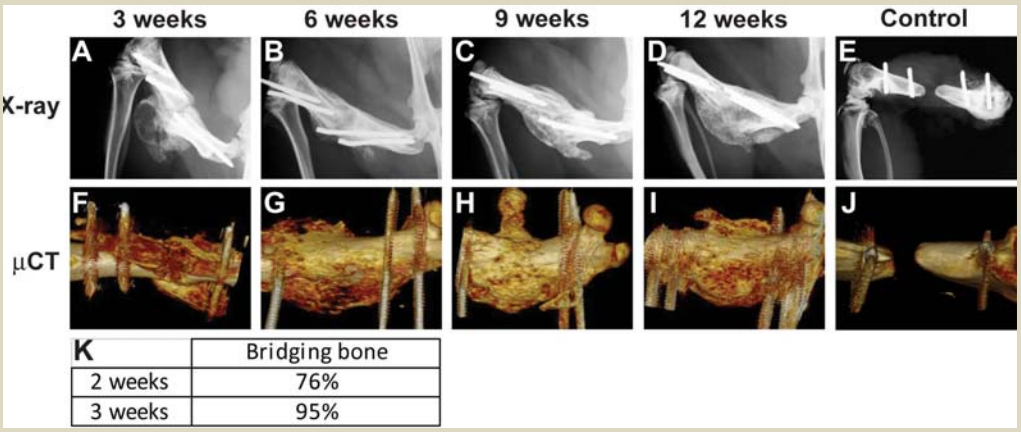

K	Bridging bone
2 weeks	76%
3 weeks	95%

Figure 32: Radiological analysis at 3, 6, 9 and 12 weeks post surgery. (A-E) X-ray images and (F-J) 3D surface renderings obtained from microcomputational analysis of the bone formation within the defect at 3 weeks (A, F), 6 weeks (B, G), 9 weeks (C, H) and 12 weeks (D, I) post surgery. Controls as a 12 weeks post surgery are shown in E and J. (K) Radiographic assessment of samples which had bone bridging the defect at 2 and 3 weeks post surgery (expressed in percentage, n=21).

Histologically, the repaired defect site exhibited mature bone filling the defect at 3 weeks (Fig. 34A). Microbeads are present at the periphery and newly formed bone is also observed around the microspheres within the defect. No inflammatory reaction was observed within the newly forming callus or tissues surrounding the microspheres. Interestingly, new bone appears to be integrated or fused with the intact femur suggesting complete bone healing and supporting the results seen by microCT. However, at 3 weeks, areas of cartilage and immature bone were observed. At this time, bone appeared to be more trabecular and less cortical, although there was the appearance of early cortical bone at the defect edges, suggesting the callus is still undergoing remodeling. At 12 weeks, no more cartilage is seen in the area of newly formed bone (Fig. 34B), and there is now a well developed cortical exterior and trabecular interior as noted in the microCT images. Although not shown in this photomicrograph there was a contiguous marrow cavity.

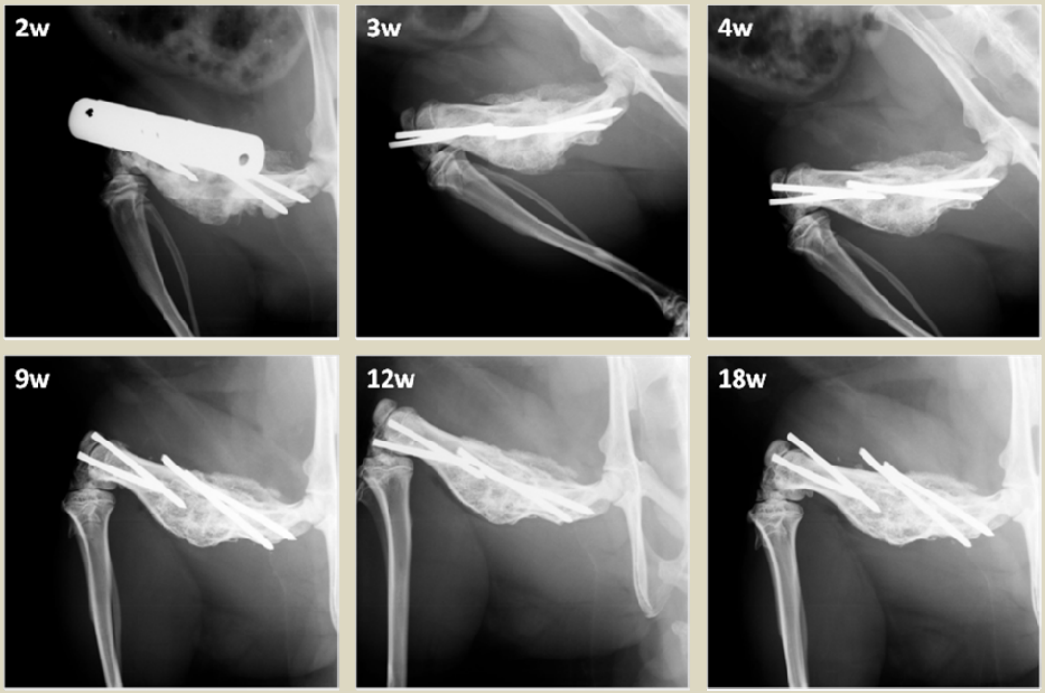

Figure 33: Longitudinal radiographic analysis of bone repair in the femoral defect model. Microspheres possessing Ad5BMP2 transduced cells were injected immediately following introduction of the 5 mm femur defect, and resultant bone healing followed over the course of 45 weeks. Bone formation appears to remodel and become more mineralized initially; (A) 2, (B) 4 and (C) 12 weeks, after which the bone was stable and did not appear undergo additional remodeling or resorption (D) 22 weeks (E) 34 weeks (F) 45 weeks post surgery.

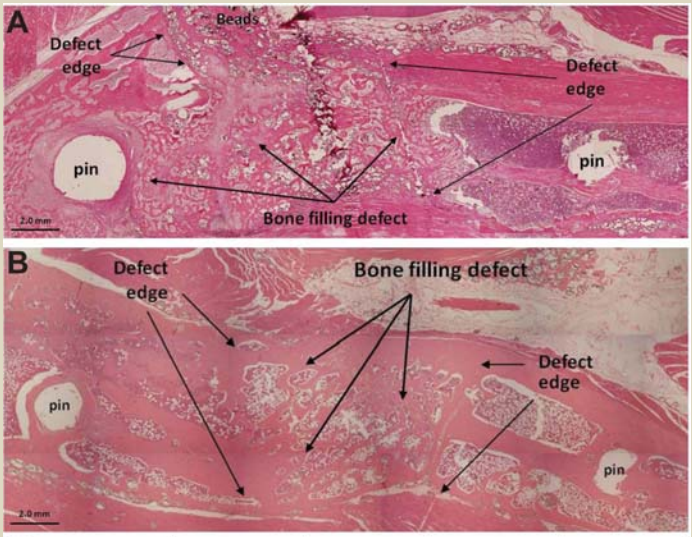

C	3 weeks	6 weeks	9 weeks	12 weeks
Cartilage	+++	+	+/-	-
New bone	++	+++	+++	+++
Marrow cavity	-	+/-	+	++

Figure 34: Histological analysis at bone repair of the femoral defect. The hind limb of interest has been harvested, formalin fixed, paraffin embedded, serial sectioned, and every 5th section stained with Hematoxylin Eosin. Representative photomicrograph of bone healing in the femoral defect at 3 weeks (A) and 12 weeks (B) post injection of osteoinductive microspheres. The photomicrograph is a montage of representative images taken at 2X magnification through the entire defect region. The defect edges are highlighted with arrows. We observed substantial amount of immature bone filling the defect. Calcified cartilage was also observed within the central callus. Holes within the femur ends represent the location of the bone pins used for the external fixation, which were removed prior to tissue processing. (C) The percentage of samples which had cartilage, immature bone, and/or presence of marrow cavity at various times after injection of osteoinductive microspheres.

Biomechanical analysis of the new bone, suggests that it rapidly obtains strength comparable to the intact femur.

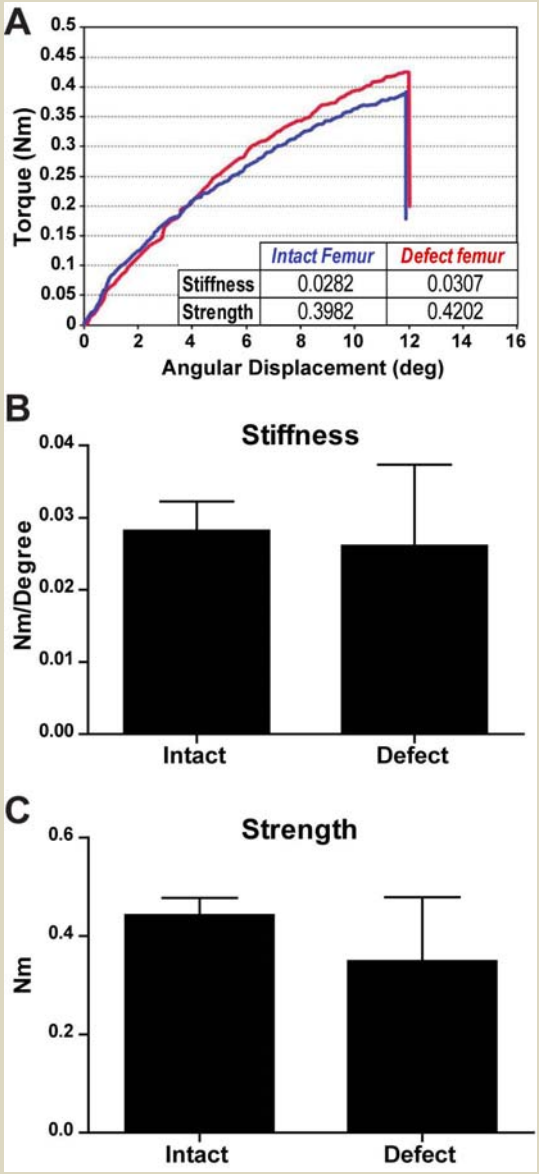

Figure 35: Biomechanical analysis of bone healing in the femoral defect model at 3 weeks post surgery. (A) Typical graphic representation of the biomechanical tests. Graphical depiction of torsional stiffness (B) and strength (C) of femur defect and intact contralateral femur. Statistical analysis (t-test) demonstrated no statistically significant difference in stiffness and strength between defect and intact femur specimens (p=0.8021 and p=0.4974, respectively; n=3).

Biomechanical torsional testing was performed on both intact and operated femurs isolated from the rats at 3 weeks post surgery. To control for variations in shape and size of the femurs between animals, the newly repaired femur was compared to the intact contralateral femur within each harvested pair. The average torsional stiffness at 3 weeks was 0.026 ± 0.011 Nm/Degree and 93% of the contralateral intact femur (Fig. 6B). The average torsional strength was 0.35 ± 0.13 Nm and 79% of the contralateral intact femur (Fig. 6C). These results showed no statistically significant difference in stiffness and strength between defect and intact femur (p=0.8021 and p=0.4974, respectively), suggesting that the repaired bone exhibits biomechanical properties similar to the contralateral intact femur. As seen in figure 36 we mounted the specimens in a manner to avoid fracture at the pin sites. The torsional strain in all cases resulted in a spiral fracture through the shaft of the bone. A representative 2 week sample is shown in figure 36.

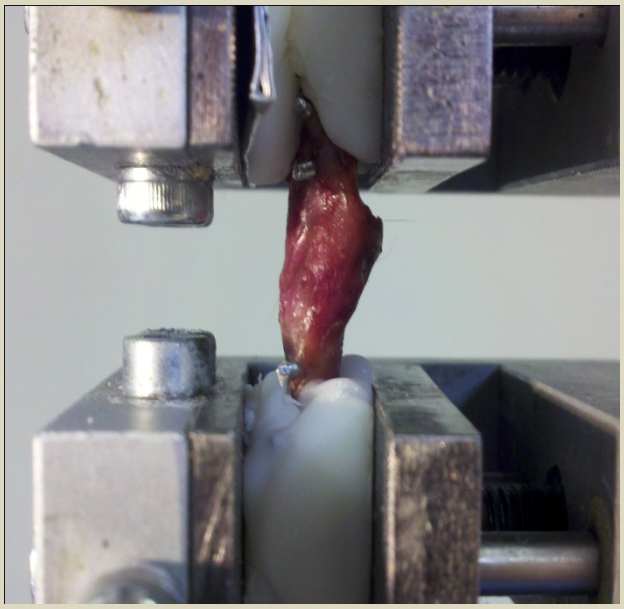

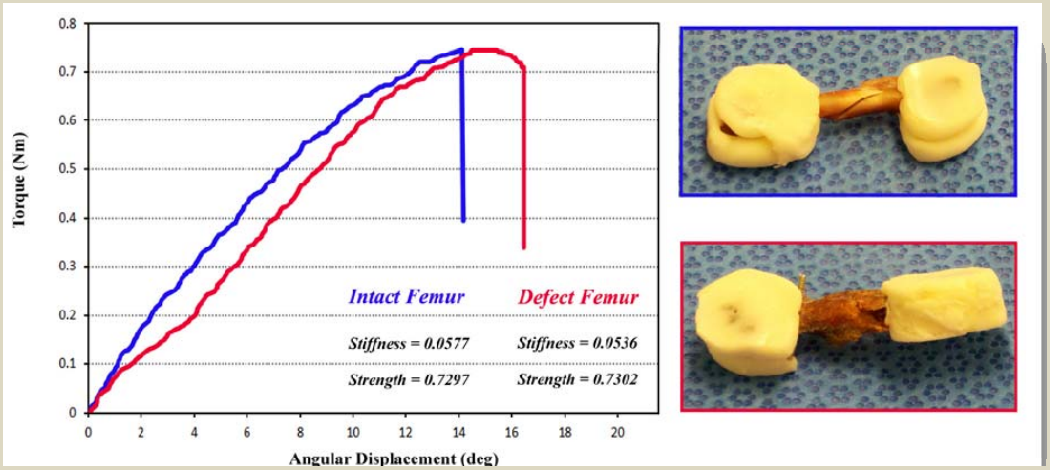

Figure 36: Representative femur undergoing torisonal strength testing. Top: femur mounted in the device. Bottom: Two week sample that fractured through a spiral fracture within the shaft.

In summary, while the new bone formed in response to our manipulation also forms structural and functional patterns that match those observed in natural healing in the absence of the non-degradable materials, it must nonetheless be a concern that unwanted persistence of any biomaterial will have long-term adverse effects on inflammation or bone composition and function. To enable us to control the fate of our system, we will incorporate cathepsin K protease sites within the hydrogel material itself. These can be recognized by osteoclasts recruited to the newly formed bone. The osteoclasts recruited into the vicinity of the new hydrogel supported bone growth will themselves cleave these sites to degrade and removal the gel material, which will then be replaced by bone.

Key Research Accomplishments:

Task 1: To produce high levels of BMP2 from human mesenchymal stem cells transduced Ad5F35BMP2 adenovirus in the presence of tetracycline carrying a red luciferase reporter gene.

- We have determined that DSRed is the most sensitive of the reporter modalities for detecting the cells in the hydrogel material after introduction into the mouse muscle.
- We have published experiments which shows that encapsulation of the transduced cells in hydrogel can extend transgene expression within the tissues. We have demonstrated a 3 fold enhancement of the bone formation with hydrogel. However, most likely the enhanced bone formation is a result of the greater volume of tissue expressing the BMP2 rather than the extended expression of the BMP.
- We have examined the tissues to for the presence of phosphoSmad and identified cells within the nerve sheath that appear to be responding to the BMP2. We then looked at both characterizing the mechanism by which the BMP2 exposure leads to bone formation, and identified a novel neural crest stem cell population. Further, blocking expansion of this population appeared to significantly reduce bone formation.
- **Studies completed in this aim have led to two publications in peer reviewed journals.**

Task 2: To design an optimal hydrogel material that will rapidly promote endochondral bone formation and be capable of removal through bone remodeling processes.

- We have constructed the cathespin K protease site, and introduced it into the hydrogel material.
- We have initially tested this material and found it to be selectively degraded by cathespin K as compared to other proteases.
- We have shown that osteoclasts will adhere, form ruffled borders, and start to resorb the material, presumably by the production of cathespin K.
- We have introduced RGD peptide binding sites to the hydrogel material to provide adhesion for the osteoclasts, as well as to extend the life span of the cells within the gel.
- We have engineered RANK ligand into the hydrogel material which can be bound by the osteoclast precursors to induce osteoclastogenesis, similar to skeletal remodeling. In normal bone remodeling RANKL is released by the osteoblasts to induced osteoclast differentiation, and resorption. Thus it will aid in allowing the biomaterial to function similar to normal bone matrix.
- We are finishing these *in vitro* experiments by demonstrating the inability of other fibroblasts to degrade the material. We have preliminary data that we are currently quantifying to demonstrate the amount of hydrogel degradation we observe in the presence of osteoclasts versus other fibroblast cells, which may adhere in the *in vivo* model.
- We have filed a disclosure and are moving to patent this material.
- **Studies have led to one publications in peer reviewed journals**
- Our next goal is to implement the material *in vivo*. In these experiments we have determined that there appears to be a maximal stimulation of BMP2 where upon addition of more BMP2 does not result in greater bone formation.
- We have optimized the hydrogel to be able to encapsulate the AdBMP2 transduced cells, and express the BMP2 at similar levels to the un-encapsulated cells. We have shown that the region of BMP2 secretion appears to dictate the area and location of the new bone formation, and when the microspheres were which due to the additional material encompass a much larger area; a much larger bone was formed. Thus the microbeads are able to target the bone to their location, which is critical for healing large defects.
- We have demonstrated the ability of the AdBMP2 transduced cells to heal the fibula through generation of *de novo* bone formation within the muscle, and that the large volume of bone originally generated resorbs quickly leaving on the HO which has integrated with the fibula bone, and remodeled to heal the structure. Since the fibula is non-weight bearing we observed significant resorption of the skeletal bone even with simple fracture. However, even in this challenging model, the AdBMP2 transduced cells were able to completely heal the bone in as little as 9 weeks.
- **This has resulted in a peer reviewed publication**.
- We have initiated testing of the degradable hydrogel in this model, and found that bone formation and degradation appeared to occur simultaneously, and will likely be able to recapitulate our findings with the unencapsulated cells. We have shown *in vitro* that osteoclasts were able to selectively degrade the polymer, whereas osteoblasts were not able to.

Task 3: To achieve rapid bone formation by percutaneous injection of the encapsulated Ad5F35BMP2 transduced human bone marrow mesenchymal stem cells (hBM-MSCs) into the adjacent musculature of athymic rats in a model of nonunion. We have now completed this aim using wild type rats. In this aim, we demonstrated that direct injection of this system into the defect, led to rapid bone formation and healing. The newly formed bone, integrated rapidly, and was biomechanically as strong as the contralateral uninjured femur. Further, histologically the bone was indistinguishable from normal skeletal bone, patterning as the normal femur. Finally we have preliminary data that suggests that if we inject the system several weeks after introduction of the defect, at a point where the bone has healed to a non-union fracture, the HO will rapidly grow, intregrate, and remodel the femur ends to completely heal the fracture.

- We have established and set up a reproducible critical size defect model that due to the nature of the site is a tremendously challenging model of bone healing.
- We have demonstrated the ability to transduce both the human cells to express high levels of BMP2, as well as the rat fibroblasts, which we believe to be genetically matched donors.
- We have found that we cannot generate heterotopic ossification in rats without placing the BMP2 transduced cells, near the skeletal bone. We have found that the only way to generate HO at a distal site is to induce HO within close proximity to the skeletal bone, and then distally, which results in HO forming in both places.***This work is a critical finding because we have now confirmed that if the skeletal bone is fractured, and then we inject BMP2 at a distance, HO will rapidly form, whereas in rats which do not possess fracture, HO will not form. This provides substantial insite into the fact that the fracture appears to launch a reaction, which can be recruited distally for bone formation, that otherwise would not occur. Further we have initially characterized the changes in the early fracture and have found that the periosteum (reacts) through remodeling of the large sensory nerve that is within this region. Another immediate change is the rapid production of brown adipose between the periosteum and cortex of the skeletal bone, suggesting that the periosteal nerve is reacting to the fracture to mobilize cells similar to the mechanism described in Task 1. This work is currently being prepared for a publication.***
- We have now demonstrated the necessity of the PEGDA hydrogel encapsulation of the AdBMP2 transduced cells for retaining the cells in the defect and for inducing rapid bone formation. In a model of critical size defect we have demonstrated the ability to heal the bone within two weeks with 80% of the animals healed by 3 weeks, as determined by torsional strength and stiffness testing of the bone.
- Histological analysis shows that the bone is clearly integrated and remodeled with well defined cortical bone throughout the defect.
- Removal of the external fixator at two weeks in a subset of animals resulted in no further fracture, in this group, and no adverse events for more than 1 year.
- The PEGDA hydrogel encapsulated AdBMP2 cell dose required for bone healing is **100-1000 fold lower** BMP2 protein than would yield bone in this model if using recombinant BMP2. Therefore sustained low level release of the protein produced in eukaryotic cells more closely resembling human cells resulted in substantially more robust bone formation, than with recombinant protein.
- **This work is currently in peer review**
- We have demonstrated that these osteoinductive microspheres, PEGDA hydrogel encapsulated AdBMP2 transduced cells, can be manufactured using an allogenic cell line. BMP2 expression levels confirmed to be approximately 50 ng of BMP2 per 10^7, and then encapsulated and cryopreserved in specific amounts, so that they could readily be shipped and retained at hospitals for rapid administration.
- Finally the newly healed femoral defect was compared biomechanically to the uninjured femur, and shown to possess similar torsional strength and stiffness. The data demonstrates the efficacy of the hydrogel microspheres to rapidly heal critical size defects.
- **This aim is completed for the first generation non-degradable form of the polymer, and close to completion with the degradable form.**

Reportable Outcomes:

Oral presentation:

- Olmsted-Davis E. A., Davis, A.R. and West, J. L. The Role of the Peripheral Nervous System in Heterotopic Ossification. Advances in Mineral Metabolism and John Haddad Young Investigators Meeting, Aspen, CO April 6-10.
- Ronke Olabisi, Corinne Sonnet, ZaWaunyka Lazard, Chartrisa Simpson, Alan Davis, Jennifer West, Elizabeth Olmsted-Davis, Hydrogel Microencapslation Permits Critical Size Defect Repair Via Gene Therapy. In Society For Biomaterials Annual Meeting and Exposition, Orlando, FL 13-16 April, 2011
- Sonnet C, Olabisi R, Sullivan K, LaShan Simpson C, Hipp J, Davis AR, West JL, and Olmsted-Davis EA. Induction of heterotopic ossification in rats requires skeletal bone. Texas Bone Disease Program of Texas. March 2011.
- Simpson, C, Sonnet C, Olabisi R, Sullivan K, Davis AR, West JL, and Olmsted-Davis EA. Osteoinductive microspheres rapidly heal a critical size defect. Tissue Engineering and Regenerative Medicine International Society (TERMIS). January 2012.

Poster presentation:

- Corinne Sonnet, Ronke Olabisi Ph.D., Kayleigh Sullivan, LaShan Simpson Ph.D., John Hipp Ph.D, ZaWaunyka Lazard, Zbigniew Gugala M.D., Ph.D., Francis Gannon M.D, Angie Fuentes, Steve Stice Ph.D, John Peroni DMV, Michael Heggeness M.D., Ph.D., Alan R. Davis Ph.D., Jennifer West Ph.D., Elizabeth Olmsted-Davis Ph.D Cell-based gene therapy for fracture healing on a rat femoral critical size defect. American Society of Bone and Mineral Research Annual Meeting San Diego, CA Oct. 2012.

- Ronke Olabisi, Corinne Sonnet, ZaWaunyka Lazard, Chartrisa Simpson, Alan Davis, Jennifer West, Elizabeth Olmsted-Davis, Critical Size Defect Repair through a Single Injection. In 57th Annual Meeting of the Orthopaedic Research Society, Long Beach, CA, 13-16 January 2011.

- Ankit Rajgariah, Ronke Olabisi, Ph. D., Lashan Simpson, Corrine Sonnet, Alan R. Davis, Elizabeth Olmsted-Davis, Jennifer West, Determining The Number of Cells Encapsulated When Making PEG-DA Hydrogel Microspheres. In Biomedical Engineering Society Annual Meeting, Austin, TX 6-9 Oct 2010.

- Ronke M Olabisi, ZaWaunyka Lazard, Mary Hall, Eva Sevick, Alan R Davis, Elizabeth A Olmsted-Davis, Jennifer L West, Hydrogel microspheres increase cell survival and increase new bone volume in a gene therapy bone formation model. In Society for Biomaterials Annual Meeting and Exposition, Seattle, WA, 21 - 24 April 2010.

- Ronke M Olabisi, Chi-Wei Hsu, Alan R Davis, Elizabeth A Olmsted-Davis, Jennifer L West, Cathepsin-K and Osteoclast Sensitive Poly(ethylene) Glycol Hydrogels. In 56th Annual Meeting of the Orthopaedic Research Society, New Orleans, LA, 6 - 10 March 2010.

- Jennifer Mumaw, Erin Jordan, Corinne Sonnet, Ronke Olabisi, Elizabeth Davis, Alan Davis, Jennifer West, Steven Stice. Cryopreservation of encapsulated therapeutic cells in a model for bone regeneration. Petit Institute for Bioengineering and Bioscience Industrial Partners Symposium. Atlanta, GA 21-22 Oct 2010.

Manuscripts Published or in Press:

- Fouletier-Dilling CF, Wada A, Lazard Z, Salisbury E, Gannon F, Vadakkan T, Gao L, Hirschi K, Dickinson M, Davis AR, Olmsted-Davis E. (2010). Vessel Formation is Induced Prior to the Appearance of Cartilage in BMP2-Mediated Heterotopic Ossification. J Bone Miner Res. J Bone Miner Res. 25(5):1147-56. PMID: 19839764

- Ronke M Olabisi, Zawaunyka Lazard, Michael Heggeness, Kevin M Moran, John A Hipp, Ashvin

Dewan, Alan R. Davis, Jennifer L. West and Elizabeth A. Olmsted-Davis. An Injectable Method for Spine Fusion. Spine J. 2011 Feb 1. [Epub ahead of print] PMID: 21292563

- Ronke M. Olabisi, ZaWaunyka Lazard, Elizabeth A. Olmsted-Davis, Alan R. Davis, Jennifer L. West. (2010). Comparison of endochrondal bone formation after delivery of a cell based gene therapy system, with and without PEG-DA hydrogel encapsulation. Tissue Engineering Part A. 16(12):3727-36. PMID: 20673027

- Chih-Wei Hsu, Ronke M. Olabisi, Elizabeth A. Olmsted-Davis, Alan R. Davis, Jennifer L. West Cathepsin-K sensitive poly(ethylene Glycol) hydrogels for degradation in response to bone formation. J Biomed Mater Res A. 2011 Apr 26. [Epub ahead of print]. PMID: 21523904

- ZaWaunyka Lazard, Jerome Saltarrelli, Christian Clarke, Michael Heggeness, Jennifer West, Alan R. Davis, and Elizabeth Olmsted-Davis. Induction of targeted heterotopic ossification for healing traumatic bone injury. J Cell Biochem. 2011 Jun;112(6):1563-71. [Epub ahead of print.] PMID:2134448

- Elizabeth Salisbury, Eric Rodenberg , Corinne Sonnet, John Hipp, Francis Gannon, Tegy Vadakkan, Aya Wada, Mary Dickinson, Elizabeth A. Olmsted-Davis, and Alan R. Davis. Sensory Nerve Induced Inflammation Contributes to Heterotopic Ossification. J Cell Biochem. 2011 Jun 15. [Epub ahead of print] PMID:21678472

- Jennifer Mumaw, Erin Jordan, Corinne Sonnet, Ronke Olabisi, Alan Davis, Jennifer West, Steven Stice, Elizabeth Olmsted-Davis. Cryopreservation of encapsulated therapeutic cells in a model for bone regeneration.

Manuscripts in Review:

- Sonnet C, Olabisi R, Simpson C, Sullivan K, Fuentes A, Hipp J, Davis AR, West JL, Olmsted-Davis EA. Rapid Healing of Femoral Defects using Osteoinductive Microspheres

- Sonnet C, Olabisi R, Sullivan K, Simpson C, Hipp J, Davis AR, West JL, and Olmsted-Davis EA. Induction of heterotopic ossification in rats requires skeletal bone.

- Gugala, Z, Sonnet, C, Simpson C., Sullivan, K., Davis, AR, West, JL, and Olmsted-Davis, EA. Biomechanical testing of femur healing in a rat model of critical size defect after injection of osteoinductive microspheres.

Conclusions:

We have completed 90 percent of the proposed studies in this application and published the findings in several peer-reviewed manuscripts. We have identified some of the earliest events in BMP2 induced bone formation, and including a novel stem cell population that with 24 hours appears to expand and migrate towards the region of BMP2. In vivo production of BMP2 through cell therapy, led to a maximum of 100-1000 fold lower protein levels which gave a significantly accelerated healing time in the rat assay as compared to the recombinant protein counterpart. Disruption of this process leads to reduction in bone formation. We have also developed a novel cell based gene therapy system which can produce bone formation at a targeted location. This system involves encapsulation of the transduced cells into microspheres, using PEGDA hydrogel. These microspheres are injectable and are retained at the injection site where they rapidly produce new bone formation. When injected into a critical size defect new bone formation was rapidly induced, and substantial enough to span the defect and provide initial stabilization.The external fixation device which stabilized the femur ends, and prevents compression, was removed in 10 wild type rats, at 2 weeks, resulting in continued bone healing, without any additional fractures in the animals. Further, these animals ambulated normally, and with no apparent lameness or reduction in activity. We have followed the bone healing in a number of these rats to 18 weeks, and found that mineralization peaked at 6 weeks, and represented complete healing both histologically as well as radiologically. We have currently completing the biomechanical – torsional testing

(stiffness, and yield strength) and assembling the manuscript specifically to demonstrate the potential rapid healing, and significant strength of the new bone within 3 weeks. We have also developed a formulation of the injectable microspheres, which can be remodeled through bone remodeling, which is recently published, and we are currently completing the testing of this material for "tuning" *in vivo*, to provide for similar bone healing, and eventual material remodeling.

With completion of this grant, we have completed the development of a material that has been shown in small animal models to be able to completely heal large defects, within 6 weeks, and have new bone spanning the defect and integrated with the femur, which can provide initial stabilization of the defect. Further removal of external fixation showed that the bone was stable enough within 2 weeks, to bear the animal's weight and normal activity without fracture. This material is injectable, can utilize allogenic cells, due to the encapsulation, and does not induce an inflammatory reaction. Further, the AdBMP2 transduced cells encapsulated in the hydrogel microspheres (Osteoinductive microspheres) can be cryopreserved without loss of efficacy, which provides substantial versatility for manufacturing, in which large batches can be produced, qualified, vialed and stored for use in clinical trials. Finally, we have moved to obtain a provisional patent on this in collaboration with Dr. West and Rice University. Two manuscripts remain in review at this point, but currently the small animal testing is complete. The next phase or extension of this work is to perform similar studies in a canine model, which is the recommended model for orthopedic devices, by the FDA, and which would complete the animal studies required for submission of an IND and translation into the clinic.

References:

1. Gowen, M., et al. (1999). Cathepsin K knockout mice develop osteopetrosis due to a deficit in matrix degradation but not demineralization. *J Bone Miner Res* 14: 1654-1663.
2. Hollberg, K., Nordahl, J., Hultenby, K., Mengarelli-Widholm, S., Andersson, G., and Reinholt, F. P. (2005). Polarization and secretion of cathepsin K precede tartrate-resistant acid phosphatase secretion to the ruffled border area during the activation of matrix-resorbing clasts. *J Bone Miner Metab* 23: 441-449.
3. Yang, F., Williams, C. G., Wang, D. A., Lee, H., Manson, P. N., and Elisseeff, J. (2005). The effect of incorporating RGD adhesive peptide in polyethylene glycol diacrylate hydrogel on osteogenesis of bone marrow stromal cells. *Biomaterials* 26: 5991-5998.
4. Fouletier-Dilling, CM. et al. (2005). Novel compound enables high-level adenovirus transduction in the absence of an adenovirus-specific receptor. *Hum Gene Ther* 16: 1287-1297.
5. Fouletier-Dilling CM, Gannon F, Olmsted-Davis EA, Lazard Z, Heggeness MH, Shafer JA, Hipp JA, and A.R. Davis. (2007) Efficient and Rapid Osteoinduction in an Immune Competent Host. Hum Gene Ther 18(8):733-45 (Fast Track publication and Cover).
6. Olmsted-Davis, EA, *et al.* (2002). Use of a chimeric adenovirus vector enhances BMP2 production and bone formation. *Hum Gene Ther* 13: 1337-1347.
7. Bikram M, Fouletier-Dilling CM, Hipp JA, Gannon F, Davis AR, Olmsted-Davis EA, and West JL (2007) Endochondral Bone Formation from Hydrogel Carriers Loaded with BMP2-Transduced Cells. Ann Biomed Eng. 35(5):796-807.
8. Olmsted, EA. *et al.* (2001). Adenovirus-mediated BMP2 expression in human bone marrow stromal cells. *J Cell Biochem* 82: 11-21.
9. Gugala, Z., Davis, A.R., Fouletier-Dilling, C, F. Gannon, Lindsey, R.W., Olmsted-Davis, EA (2007) Adenovirus BMP2-Induced Osteogenesis in combination with various collagen carriers. Biomaterials, 28(30):4469-79.